

An Optimally-Tuned Starting Point for Single-Shot GW Calculations of Solids

Stephen E. Gant,¹ Jonah B. Haber,¹ Marina R. Filip,² Francisca Sagredo,¹
Dahvyd Wing,³ Guy Ohad,³ Leeor Kronik,³ and Jeffrey B. Neaton^{1,4,5,*}

¹*Department of Physics, University of California Berkeley, Berkeley, California 94720, USA*

²*Department of Physics, University of Oxford, Clarendon Laboratory, Oxford OX1 3PU, United Kingdom*

³*Department of Molecular Chemistry and Materials Science,
Weizmann Institute of Science, Rehovoth 76100, Israel*

⁴*Materials Sciences Division, Lawrence Berkeley National Laboratory, Berkeley, California 94720, USA*

⁵*Kavli Energy NanoScience Institute at Berkeley, Berkeley, California 94720, USA*

The dependence of *ab initio* many-body perturbation theory within the GW approximation on the eigensystem used in calculating quasiparticle corrections limits this method’s predictive power. Here, we investigate the accuracy of the recently developed Wannier-localized optimally tuned screened range-separated hybrid (WOT-SRSH) functional as a generalized Kohn-Sham starting point for single-shot GW (G_0W_0) calculations for a range of semiconductors and insulators. Comparison to calculations based on well-established functionals, namely, PBE, PBE0, and HSE, as well as to self-consistent GW schemes and to experiment, shows that band gaps computed via $G_0W_0@WOT-SRSH$ have a level of precision and accuracy that is comparable to that of more advanced methods such as quasiparticle self-consistent GW and eigenvalue self-consistent GW . We also find that $G_0W_0@WOT-SRSH$ improves the description of states deeper in the valence band manifold. Finally, we show that $G_0W_0@WOT-SRSH$ significantly reduces the sensitivity of computed band gaps to ambiguities in the underlying WOT-SRSH tuning procedure.

I. INTRODUCTION

Ab initio many-body perturbation theory within the GW approximation is a state-of-the-art approach for calculations of the quasiparticle (QP) band structures of crystalline solids [1–16]. In the GW approximation, the self-energy Σ is given by the convolution $\Sigma = iGW$, where G is the single particle Green’s function and W is the dynamically screened Coulomb interaction. The GW self-energy is normally first constructed from a (generalized) Kohn-Sham (GKS) [17] “starting point”, an eigensystem computed from density functional theory (DFT). While semi-local functionals, such as the local density approximation [18] or generalized gradient approximations like PBE [19], have historically been the standard choice for constructing this starting point eigensystem [5, 8, 9, 11], hybrid functionals are increasingly used [16, 20–28].

In practice, there are a variety of choices regarding how GW calculations are carried out, with significant consequences for accuracy [16, 29]. Once the GW self-energy has been constructed, the quasiparticle energies can be computed via first-order correction to the GKS eigenvalues, the so-called single-shot GW (G_0W_0) approach [5], or G and/or W can be iterated to self-consistency [21, 22, 24–26, 28, 30–50]. The G_0W_0 method is the computationally least expensive approach, and, as has been well established, the quasiparticle band structures computed with G_0W_0 approaches typically substantially improve agreement with experiment compared to those obtained directly from the GKS eigenvalues of their underlying DFT starting points [16, 20, 44, 49, 51]. For example, QP band gap data from an analysis of G_0W_0

calculations for various semiconductors and insulators by Grumet et al. [49] exhibited a mean absolute error (MAE) of 0.2 eV compared to an MAE of 1.2 eV for the underlying DFT functionals used. However, G_0W_0 results exhibit a starting-point dependence, where results can depend considerably on the DFT functional used to construct the starting eigensystem [12, 16, 20, 27, 52]. For molecules, a range of about 1 eV in G_0W_0 calculations of highest occupied molecular orbital energies has been reported [53, 54]. Likewise, G_0W_0 results for solids (e.g., Si, InN, ZnO, ZnS, CdS, and GaN) [20, 55] have shown a similar starting point dependence of up to 2 eV in computed band gaps. As such, it is common practice to differentiate G_0W_0 calculations by the functional used in their starting point, denoted by $G_0W_0@(\dots)$. Relatedly, the accuracy of G_0W_0 calculations based on semi-local DFT functionals is known to depend on a fortuitous and sometimes unreliable cancellation of error between the lack of consideration of vertex corrections, which tends to cause under-screening in W_0 , and the systematic underestimation of band gaps computed from semi-local functionals, which tends to cause over-screening [35, 36].

One way to address the issue of starting point dependence is to construct the self-energy in a more self-consistent manner, leading to the development of methods like eigenvalue self-consistent GW (ev GW) [6, 32, 35] and quasiparticle self-consistent GW (QSGW) [33, 34, 36]. In ev GW , the eigenvalues used to construct G and W are iterated to self-consistency. Though ev GW is noticeably less dependent on the starting point used, the wave functions used in constructing G and W are not updated in this approach, leading to a residual modest starting point dependence (e.g., 0.4 eV in the case of azabenzenes [53]). On the other hand, QSGW seeks to variationally minimize the difference between the self-energy and a static nonlocal potential by updating both

* Corresponding author: jboneaton@lbl.gov

the wave functions and eigenvalues used to construct G and W and has been shown to be mostly independent of the starting point used [56] (though there do exist questions as to whether this holds true for some metal oxides [57, 58]). While iterating on G and/or W provides more consistent results, it also requires greater computational resources. Additionally, while the self-consistent correction of the QP eigenvalues accounts for the error due to DFT band gap underestimation in these methods, it does not systematically account for the lack of vertex corrections, leading to under-screening and larger QP band gaps [35, 37]. For example, Grumet et al. report that *evGW* and *QSGW* overestimate QP gaps by 1.0 eV and 0.8 eV on average, respectively [49].

While *GW* self-consistency schemes can reduce the starting-point dependence of G_0W_0 , the increased cost of going beyond G_0W_0 has incentivized the development of starting points for G_0W_0 calculations which do not suffer from the same level of starting-point dependence [20–22, 24, 25, 27, 28, 55]. In particular, hybrid DFT functionals, which include exact exchange, are an appealing candidate for improved G_0W_0 starting points for multiple reasons. For example, the GKS band gaps computed with these functionals vary with the amount of exact exchange present, and therefore can be used to remedy the over-screening due to band gap underestimation that is present in semi-local functionals [16]. Moreover, hybrid functionals can better address the starting point dependence associated with more localized d states [35, 55, 59], where self-interaction errors present in semi-local functionals are more pronounced [60] and lead to spurious orbital energy ordering that can propagate to the *GW* eigenspectrum [16]. In such cases, the presence of exact exchange can help to reduce this error [21, 28, 53, 55, 61, 62].

The use of hybrid functionals like PBE0 [63] and HSE [64] as starting points for G_0W_0 calculations has been shown to generally improve agreement with experiment [20, 27]. Moreover, some hybrid functionals can be tuned [65] to satisfy the ionization potential (IP) theorem [66, 67], suggesting the possibility of a more physically accurate and consistent starting point eigensystem. Specifically, Wing et al. [68] developed a procedure for parametrizing a class of screened range-separated hybrid (SRS) functionals capable of accurately predicting the band gaps of solid state materials without empirical parameters, directly from density functional theory. The parametrization is arrived at by capturing the asymptotic limit of the screened exchange potential and by using an ansatz based on the IP theorem which applies to localized Wannier functions in systems with periodic boundary conditions [69]. This class of Wannier-localized optimally tuned screened range-separated hybrid (WOT-SRS) functionals has been recently used to calculate the fundamental band gaps of semiconductors and insulators, leading to excellent agreement with experiment, with an MAE of 0.1 eV [68].

For molecules, the use of optimally tuned range-separated hybrid functionals which enforce the IP theo-

rem as a starting point for G_0W_0 , as suggested in [23], has been shown to be successful [25, 42, 43, 47, 70, 71]. However, as of yet, there has not been an analogous exploration of these non-empirical WOT-SRS starting points which approximately satisfy the IP theorem for G_0W_0 calculations of solid-state systems.

Here, we undertake such an exploration and analyze the performance of single-shot G_0W_0 @WOT-SRS calculations. For a series of 15 semiconductor and insulators, we construct G_0 and W_0 using WOT-SRS and compute band gaps as well as properties associated with states deeper in the valence band manifold such as valence bandwidths and d band positions. We then compare results with experiments and calculations from other DFT starting points. We also discuss how G_0W_0 corrections affect the sensitivity of computed bands gaps to ambiguities in the WOT-SRS tuning procedure. Overall, our calculations demonstrate that a G_0W_0 @WOT-SRS approach provides accurate quasiparticle properties for a broad range of materials, opening the door to predictive single-shot G_0W_0 calculations for chemically complex solids.

II. THEORY

II.1. DFT

The starting point for our *GW* calculations are GKS orbitals $\phi_{n\mathbf{k}}$ and eigenenergies $\epsilon_{n\mathbf{k}}^0$, where n is the band index and \mathbf{k} the wave vector. Here, we primarily focus on the SRS functional scheme [39, 72–74]. This class of functionals is formulated by partitioning the exchange portion of the Coulomb potential into

$$\frac{1}{r} = \frac{\alpha + \beta \text{erf}(\gamma r)}{r} + \frac{1 - [\alpha + \beta \text{erf}(\gamma r)]}{r}. \quad (1)$$

This partition introduces three parameters α , β , and γ , the physical and computational significance of which is discussed shortly. When implemented in the hybrid functional, the first term of Eq. (1) is treated explicitly with Fock exchange, whereas the second term is replaced with an approximate semi-local exchange functional [39, 72]. In this framework, α regulates the amount of exact exchange in the short range, $\alpha + \beta$ regulates the amount of exact exchange in the long range, and γ is the length scale for the transition between these two limits. The correlation component is treated with the same functional used for the semi-local part of the aforementioned exchange partition. By specifying the values of α , $\alpha + \beta$, and γ , we can recover various well-known hybrid functionals (Table I). For example, if the semi-local exchange is based on the PBE functional [19], then setting $\gamma = 0$ produces a global hybrid functional, PBE α [75, 76], and if $\alpha = 0.25$, PBE0 is obtained. For $\gamma = 0.106 a_0^{-1}$, setting $\alpha + \beta = 0$ and $\alpha = 0.25$ yields the HSE functional [64].

In this paper, we focus on the novel WOT-SRS formulation [68] of the SRS functional. Here, the choice $\alpha + \beta = \epsilon_{\infty}^{-1}$, where ϵ_{∞}^{-1} is the orientationally averaged

	α	$\alpha + \beta$	γ (a_0^{-1})
PBE0	0.25	0.25	0
HSE06	0.25	0	0.106
WOT-SRSH	Varies ^a	ε_∞^{-1}	Tuned

TABLE I. Hybrid functionals in the SRSH formalism
a: By default α is set to be 0.25, but in cases where $\alpha + \beta \sim 0.25$ the value of α is increased slightly until the IP ansatz can be satisfied. For more details see [68] or the discussions in sections II.1 and IV.2.

electronic contribution to the dielectric constant, enforces the asymptotically correct long-range screening in the Coulomb potential [39, 73, 74]. The range-separation parameter γ is non-empirically selected by enforcing an ansatz which extends the IP theorem to the removal of an electron from the highest-energy occupied maximally-localized Wannier function (MLWF) [69]. By default, we choose $\alpha = 0.25$ because, as seen in global hybrids, setting $\alpha = 0.25$ has proven effective for many molecular and solid-state systems [41, 75, 77, 78]. In cases where setting $\alpha = 0.25$ does not yield a unique choice of γ via the IP ansatz, as is often the case when $\varepsilon_\infty^{-1} \sim 0.25$, α is increased slightly until an optimal value of γ that does not approach zero can be found. The need for a lower bound on the size of γ is related to the “ γ collapse problem” [79, 80], where small values of γ result in an unphysical effectively PBE α hybrid functional if γ^{-1} exceeds the size of the unit cell of the calculation. As seen in Table II, the largest value that α needed to be increased to was 0.35. With these constraints, WOT-SRSH functionals are a system-specific but non-empirical class of exchange correlation (xc) functionals that result in a GKS eigensystem that consistently and accurately predicts the QP

band gaps of solids, compensating by construction for the derivative discontinuity error present in most density functionals [11, 17, 81–86].

II.2. GW Method

In the *ab initio* GW approach, the self-energy $\Sigma = iGW$ of a system is constructed from a DFT GKS eigensystem. As discussed, this GKS eigensystem $\{\phi_{n\mathbf{k}}, \epsilon_{n\mathbf{k}}^{\text{DFT}}\}$ depends on the underlying xc functional V_{xc} used to compute it, and by extension the self-energy computed from this eigensystem is also sensitive to the choice of V_{xc} . Specifically, the single-particle Green’s function G_0 is constructed as

$$G_0(\mathbf{r}, \mathbf{r}'; \omega) = \sum_{n\mathbf{k}} \frac{\phi_{n\mathbf{k}}(\mathbf{r})\phi_{n\mathbf{k}}^*(\mathbf{r}')}{\omega - \epsilon_{n\mathbf{k}}^{\text{DFT}} \pm i\eta}, \quad (2)$$

where η is a positive infinitesimal real number, and the \pm in front of it is $-$ for occupied states and $+$ for empty states. The dynamically screened Coulomb interaction W_0 is given by

$$W_0(\mathbf{r}, \mathbf{r}'; \omega) = \int d\mathbf{r}'' \varepsilon^{-1}(\mathbf{r}, \mathbf{r}''; \omega) v(\mathbf{r}', \mathbf{r}''), \quad (3)$$

where $v(\mathbf{r}, \mathbf{r}') = |\mathbf{r} - \mathbf{r}'|^{-1}$ and where the dielectric function,

$$\varepsilon^{-1}(\mathbf{r}, \mathbf{r}'; \omega) = \delta(\mathbf{r}, \mathbf{r}') - \int d\mathbf{r}'' v(\mathbf{r}, \mathbf{r}'') \chi_0(\mathbf{r}'', \mathbf{r}', \omega), \quad (4)$$

is computed within the random-phase approximation (RPA) [6] based on the polarizability $\chi_0(\mathbf{r}, \mathbf{r}', \omega)$, given by the Adler-Wiser expression [87, 88]

$$\chi_0(\mathbf{r}, \mathbf{r}', \omega) = \sum_{n\mathbf{k}} \sum_{n'\mathbf{k}'}^{\text{occ. emp.}} \left[\frac{\phi_{n\mathbf{k}}^*(\mathbf{r})\phi_{n'\mathbf{k}'}(\mathbf{r})\phi_{n\mathbf{k}}^*(\mathbf{r}')\phi_{n'\mathbf{k}'}(\mathbf{r}')}{\omega - (\epsilon_{n'\mathbf{k}'}^{\text{DFT}} - \epsilon_{n\mathbf{k}}^{\text{DFT}}) + i\eta} - \frac{\phi_{n\mathbf{k}}(\mathbf{r})\phi_{n'\mathbf{k}'}^*(\mathbf{r})\phi_{n\mathbf{k}}(\mathbf{r}')\phi_{n'\mathbf{k}'}^*(\mathbf{r}')}{\omega + (\epsilon_{n'\mathbf{k}'}^{\text{DFT}} - \epsilon_{n\mathbf{k}}^{\text{DFT}}) - i\eta} \right], \quad (5)$$

where the summations are over the occupied and unoccupied bands. In practice, $\chi_0(\mathbf{r}, \mathbf{r}', \omega)$ is often evaluated statically ($\omega = 0$), and a simplified model frequency dependence, such as a plasmon pole model (PPM), is used instead [6, 89, 90]. We also note that a consideration of the denominators in Eq. (5) clarifies why the under- or overestimation of the band gap can result in over- or under-screening in W_0 , respectively.

With the above quantities, the G_0W_0 self-energy becomes

$$\Sigma(\mathbf{r}, \mathbf{r}'; \omega) = \frac{i}{2\pi} \int d\omega' G_0(\mathbf{r}, \mathbf{r}'; \omega + \omega') W_0(\mathbf{r}, \mathbf{r}'; \omega') \times e^{i\omega'\eta}. \quad (6)$$

This G_0W_0 operator can then be used to correct the DFT

eigenvalues perturbatively via

$$\epsilon_{n\mathbf{k}}^{\text{QP}} = \epsilon_{n\mathbf{k}}^{\text{DFT}} + \langle n\mathbf{k} | \Sigma(\epsilon_{n\mathbf{k}}^{\text{QP}}) - V_{xc} | n\mathbf{k} \rangle, \quad (7)$$

where, to avoid double counting of beyond-Hartree interactions, the contributions of V_{xc} are subtracted off. Due to the fact that $\epsilon_{n\mathbf{k}}^{\text{QP}}$ in Eq. (7) depends on itself, evaluating this expression is non-trivial. However, as is common practice [91–93], we expand Eq. (7) to first order about $\epsilon_{n\mathbf{k}}^{\text{DFT}}$ to evaluate it efficiently.

	Lattice Parameters			WOT-SRSH Parameters ^d		
	<i>a</i>	<i>c</i>	<i>u</i>	α	β	γ (a_0^{-1})
InSb	6.48 ^a			0.25	-0.1745	0.17
InAs	6.06 ^a			0.25	-0.1623	0.16
Ge	5.66 ^a			0.25	-0.1824	0.19
GaSb	6.1 ^a			0.25	-0.1733	0.19
Si	5.43 ^a			0.25	-0.1611	0.24
InP	5.87 ^a			0.25	-0.1373	0.23
GaAs	5.65 ^a			0.25	-0.1549	0.15
AlSb	6.14 ^a			0.25	-0.1482	0.14
AlAs	5.66 ^a			0.3	-0.1779	0.18
GaP	5.45 ^a			0.25	-0.1375	0.21
AlP	5.47 ^a			0.25	-0.1128	0.16
C	3.57 ^a			0.3	-0.1198	0.23
AlN	3.11 ^a	4.98 ^a	0.3821 ^c	0.35	-0.1073	0.26
MgO	4.22 ^a			0.25	0.0948	1.5
LiF	4.03 ^b			0.25	0.2681	1.08

TABLE II. Parameters used in the DFT starting point calculations. Lattice parameters were taken from experiment, and WOT-SRSH parameters were taken from prior work [68]. a: [94], b: [95], c: [96], d: [68]

III. COMPUTATIONAL DETAILS

III.1. DFT Calculations

Our DFT calculations are performed using a modified version of the QUANTUM ESPRESSO (version 6.2) plane-wave code [97–99] that allows for the use of the SRSH functional [39] of Eq. (1) with arbitrary α , β , and γ parameters. Other modifications also allow for a more efficient calculation of many hundreds of unoccupied states for GKS systems using adaptively compressed exchange [100] via what amounts to a non-self-consistent field calculation once the occupied orbitals and ground state density have been converged (see SI Section S-I [101] for more details). All calculations utilize fully relativistic optimized norm-conserving Vanderbilt pseudopotentials [102] obtained from the PSEUDO-DOJO repository [103]. Using these pseudopotentials, the effects of spin-orbit coupling (SOC) are included self-consistently at the DFT level for all calculated observables. For Ge, Ga, In, Sb, and As, the electrons within a complete set of semi-core shells of the same principal quantum number are treated as valence electrons. For calculations using hybrid functionals and the *GW* methods, the explicit consideration of these deeper states has been shown to be necessary for the accurate description of the electronic structure of such systems [32, 104–106]. A plane wave energy cutoff of 135 Ry and experimental room temperature lattice parameters (summarized in Table II) are used for all systems.

For hybrid functionals, the energy cutoff involved in

constructing the exact exchange operator is lowered, without significantly impacting the results at the DFT or $G_0W_0@DFT$ levels, from its default value of four times the plane wave energy cutoff to 150 Ry. In some rare cases where this causes numerical instability in the self-consistent evaluation of the exchange, namely computing the PBE0 starting points for Ge and InAs, this cutoff is raised to the default value of four times the plane wave energy cutoff.

III.2. *GW* Calculations

All our *GW* calculations are carried out using the BERKELEYGW package [6, 107]. In an effort to minimize the cost of computing many hundreds of unoccupied states using hybrid functionals, the dielectric function is constructed using a symmetry-reduced unshifted Monkhorst-Pack \mathbf{q} grid. Frequency dependence in the dielectric function is included approximately via the Godby-Needs PPM [89, 90], which has been shown to reproduce the computed band gaps of full-frequency integration at reduced cost [108]. It should be noted, however, that this comparable level of accuracy can wane for deeper valence states; previous studies [109, 110] report that valence bandwidths and *d* band binding energies computed using the Godby-Needs PPM are modestly overestimated relative to full-frequency integration.

The static remainder approximation to Σ [111] is used whenever it yields faster convergence with respect to the number of bands, which is the case for all materials except AlN, MgO, and LiF. The band gaps of all materials are converged within (or well within) 50 meV with respect to the number of bands used to construct ϵ and Σ , the energy cutoff in the construction of ϵ , and the unshifted \mathbf{k} grid being used. For more convergence details, see SI Section S-II [101].

The effects of SOC are computed at the DFT level and added perturbatively at the G_0W_0 level for all materials, an approximation which has precedent and justification for the classes of materials under study [112–114]. While BERKELEYGW does allow for the explicit computation of SOC effects at the *GW* level, this would require twice as many bands in the starting point eigensystem, quadrupling the cost of already expensive calculations. However, we find the error of including SOC perturbatively to be minimal. For example we report that for AlSb, a system with a strong SOC band gap renormalization of 240 meV, the error in the computed SOC renormalization of the band gap is only 6 meV. For systems with weaker renormalizations like GaP, this error is only 1 meV.

For band structures with conduction band minima off high symmetry points (as is the case for Si, C, GaP, and AlSb), eigenvalues are interpolated using the WANNIER90 code [115]. Due to the similarity in orbital character of the states near the band gap for all the aforementioned systems, only the four highest occupied and four lowest unoccupied bands about the band edges are Wannierized, with sp^3 starting projections being used for

all of them. SOC corrections to the interpolated bands are determined for each eigenenergy $\epsilon_{n\mathbf{k}}$ and interpolated using MLWFs, as outlined by Malone and Cohen [112].

IV. RESULTS AND DISCUSSION

IV.1. Quasiparticle Band Structures

IV.1.1. Band Gaps

The QP band gaps of 15 semiconductors and insulators calculated from WOT-SRSH, as well as G_0W_0 using four starting points (PBE, PBE0, HSE06, and WOT-SRSH), are given in Table III and graphed in Figure 1. Additional results from DFT functionals other than WOT-SRSH can be found in the SI, section S-III.A [101]. While zero point renormalization (ZPR) effects due to electron-phonon coupling have a significant impact on the band gaps of many solids [124–128], they are not addressed computationally in this paper. Instead, computed band gaps are compared to reference band gaps which remove ZPR effects from the experimental measurements (see [68]). Additionally, excitonic effects are accounted for in our reference set by adding estimated or calculated exciton binding energies to the measured optical absorption edge or by inferring the fundamental band gap position based on the location and identification of excitonic absorption peaks in experimental data (See [68] for more details).

In line with what we have reported previously [68], the WOT-SRSH functional yields an excellent MAE of 0.07 eV and a mean signed error (MSE) of 0.00 eV for band gaps—the highest accuracy of all of the methods under study for this set of solids. As the MSE indicates, the data are nearly equally spread between over- and underestimating band gaps. Also, unlike the other functionals, WOT-SRSH has accuracy that is maintained for wider-band gap systems and has a much smaller maximum magnitude error of 0.2 eV.

Performing G_0W_0 based on the WOT-SRSH starting point for this set of materials yields an MAE of 0.19 eV, with the G_0W_0 @WOT-SRSH calculated band gaps maintaining a similar level of precision with a maximum error of 0.40 eV. Notably, the G_0W_0 @WOT-SRSH band gaps are all slightly overestimated, consistent with the overestimation observed with more rigorously self-consistent methods such as *evGW* and *QSGW* [34, 37, 48, 49] (see table III and Figure 1). Some of the reported overestimation for these methods has been attributed to the absence of ZPR effects in the band gap [34, 37], but our reference band gap accounts for ZPR effects and still indicates some systematic overestimation. However, it is also known that the RPA dielectric function can under-screen and thus overestimate band gaps. As previously noted [37, 45, 48, 129–131], beyond-RPA vertex corrections for a similar set of semiconductors and insulators can provide an improvement in the accuracy of the screening and QP band gaps once a consistent starting point that no

longer underestimates the band gap is reached.

Comparing G_0W_0 @WOT-SRSH to self-consistent *GW* approaches in Figure 1, we find excellent agreement and superior performance relative to experiment for the systems studied here, at a lower computational cost. G_0W_0 @WOT-SRSH also has a similar qualitative performance to these methods, consistently modestly overestimating band gaps across a broad range of materials.

As is well known and in agreement with prior work [16, 20, 44, 49, 51], G_0W_0 @PBE significantly improves the accuracy of PBE band gaps, in this case bringing its MAE from 1.5 to 0.4 eV. G_0W_0 @PBE also corrects major qualitative issues such as the inverted band gaps of InSb, InAs, and GaSb. Notably, however, band gaps of some insulators are still underestimated by more than 1 eV (e.g. MgO, LiF) by G_0W_0 @PBE, leading to a substantial max error of -1.77 eV.

For the insulators studied (C, AlN, MgO, and LiF) we find that well-established hybrid functionals such as HSE and PBE0 offer a significant improvement over PBE as starting points for G_0W_0 calculations. However, these hybrids perform slightly worse than PBE for the remaining semiconductors. Overall, for G_0W_0 @PBE0, we observe a MAE of 0.31 eV, an MSE of 0.19 eV, and a max error of -0.60 eV. The smaller MSE relative to the MAE reflects that the band gaps computed from G_0W_0 @PBE0 switch from being overestimated for small-band-gap semiconductors to being underestimated for wide-band-gap insulators.

In the case of G_0W_0 @HSE, calculated QP band gaps have an MAE of 0.22 eV and an MSE of 0.04 eV. This comparatively near-zero MSE reflects that the band gaps computed from G_0W_0 @HSE switch from being overestimated for small-band-gap semiconductors to being underestimated for wide-band-gap insulators. Moreover, while the MAE calculated for G_0W_0 @HSE is quite low and comparable to what is seen for G_0W_0 @WOT-SRSH, the performance of G_0W_0 @HSE is not consistent. For wide-band-gap insulators such as LiF, G_0W_0 @HSE underestimates the band gap by nearly 1 eV, leading to a max error of -0.80 eV.

IV.1.2. Band Structure

In Figure 2 we plot the calculated band structures from WOT-SRSH and G_0W_0 @WOT-SRSH for GaAs. Apart from a small shift, the bands are nearly identical. Additionally, the similarity of their curvature, especially near the band gap can be seen in the lower inset plot. G_0W_0 @WOT-SRSH corrections do, however, result in a flattening of the valence bands compared to those of WOT-SRSH. This can be seen in the top figure, where the lowest valence band from WOT-SRSH is ~ 0.5 eV lower than its G_0W_0 @WOT-SRSH counterpart. This indicates that away from the band gap, there may be more significant differences between bandstructures of G_0W_0 @WOT-SRSH and WOT-SRSH. In sections IV.1.3 and IV.1.4 we analyze these differences in greater detail.

	$G_0W_0@$ PBE	$G_0W_0@$ PBE0	$G_0W_0@$ HSE	WOT-SRSH	$G_0W_0@$ WOT-SRSH	evGW	QSGW	Ref	Expt, ZPR
InSb	0.09	0.58	0.45	0.32	0.44	0.79 ^a	0.61 ^a	0.19	0.17 ^e , 0.02 ^j
InAs	0.13	0.68	0.50	0.42	0.48	—	0.66 ^c	0.37	0.35 ^e , 0.02 ^j
Ge	0.47	0.91	0.78	0.69	0.74	0.95 ^b	0.95 ^c	0.71	0.66 ^f , 0.05 ^j
GaSb	0.46	1.00	0.88	0.69	0.86	—	1.15 ^c	0.76	0.73 ^e , 0.03 ^j
Si	1.18	1.57	1.42	1.14	1.40	2.18 ^a	1.49 ^a	1.18	1.12 ^f , 0.06 ^j
InP	1.41	1.96	1.81	1.56	1.80	1.97 ^a	1.64 ^a	1.40	1.35 ^e , 0.05 ^j
GaAs	1.01	1.59	1.46	1.41	1.48	1.85 ^b	1.96 ^c	1.47	1.42 ^e , 0.05 ^j
AlSb	1.51	1.90	1.74	1.71	1.78	2.61 ^a	2.22 ^a	1.65	1.61 ^e , 0.04 ^j
AlAs	2.04	2.49	2.33	2.25	2.41	2.98 ^a	2.84 ^a	2.20	2.16 ^e , 0.04 ^j
GaP	2.34	2.75	2.60	2.39	2.61	2.77 ^a	2.67 ^a	2.35	2.27 ^e , 0.08 ^j
AlP	2.44	2.92	2.75	2.52	2.82	3.2 ^a	2.94 ^a	2.51	2.49 ^e , 0.02 ^j
C	5.58	5.95	5.82	5.76	5.92	6.41 ^a	6.43 ^a	5.85	5.47 ^g , 0.38 ^k
AlN	5.72	6.55	6.35	6.56	6.69	—	6.80 ^c	6.52	6.14 ^e , 0.38 ^k
MgO	6.96	8.07	7.99	8.16	8.62	9.53 ^a	9.58 ^a	8.36	7.83 ^h , 0.53 ^l
LiF	13.58	14.75	14.55	15.34	15.63	15.90 ^b	16.63 ^d	15.35	14.20 ⁱ , 1.15 ^l
MAE	0.40	0.31	0.22	0.07	0.19	0.66 ^m	0.51		
MSE	-0.40	0.19	0.038	0.003	0.19	0.66 ^m	0.51		
Max Error	-1.77	-0.60	-0.80	-0.20	0.40	1.17 ^m	1.28		

TABLE III. QP band gaps (in eV) at the WOT-SRSH and $G_0W_0@$ DFT level for the various compounds and functionals under study. At the bottom of the table are the MAE (mean absolute error), MSE (mean signed error), and Max Error; all are in eV and measured relative to the reported reference values, which are arrived at by incorporating ZPR corrections into experimental band gap data. Experimental results are arrived at via an analysis of optical absorption spectroscopy data, where excitonic effects are taken into account to arrive at the fundamental gap (see [68] for details).

a: [49], b: [37], c: [34], d: [48], e: [116], f: [94], g: [117], h: [118], i: [119], j: [120], k: [121], l: [122, 123]

m: The MAE, MSE, and Max Error for evGW were computed using the available data for 12 out of 15 compounds.

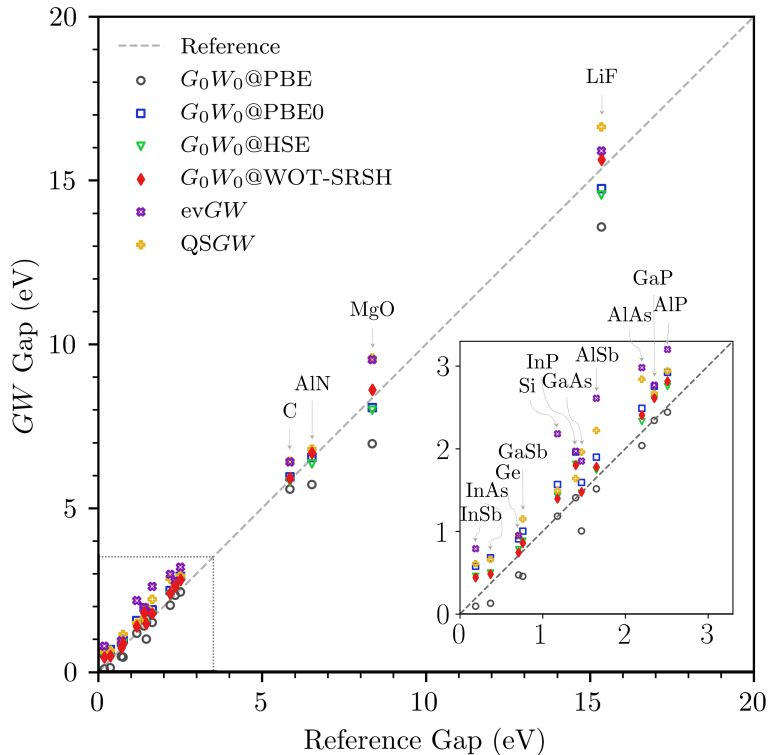


FIG. 1. QP band gaps computed using $G_0W_0@$ PBE, $G_0W_0@$ PBE0, $G_0W_0@$ HSE, $G_0W_0@$ WOT-SRSH, evGW, and QSGW in reference to ZPR corrected experimental results. Data are taken from table III. The inset in the lower right corner is a zoom-in of the bottom 3 eV of the data set.

	$G_0W_0@$	$G_0W_0@$	$G_0W_0@$	WOT-SRSH	$G_0W_0@$	Expt.
	PBE	PBE0	HSE		WOT-SRSH	
InSb	11.30	11.51	11.32	11.96	11.32	11.7 ^a (XPS), 10.8 ^a (ARPES)
InAs	11.90	12.42	12.34	13.08	12.34	12.3 ^a (XPS)
Ge	12.82	13.52	13.30	14.04	13.26	12.6 ^a (XPS)
GaSb	11.74	12.36	12.16	12.83	12.13	11.6 ^a (XPS), 11.64 ^a (ARPES)
Si	11.51	12.32	12.10	13.07	12.04	12.5 ^a (XPS)
InP	11.22	11.93	11.72	12.60	11.72	11.0 ^a (XPS), 11.4 ^a (IPES)
GaAs	12.77	13.45	13.26	14.09	13.29	13.8 ^a (XPS), 13.1 ^a (ARPES)
AlSb	10.67	11.36	11.14	12.06	11.20	—
AlAs	11.64	12.39	12.17	13.35	12.29	—
GaP	12.18	12.92	12.70	13.70	12.71	12.5 ^a (ARPES)
AlP	11.00	11.83	11.59	12.75	11.67	—
C	22.23	23.23	23.04	24.02	23.25	21 ^a (XPS)
AlN	6.55	6.73	6.69	6.65	6.75	—
MgO	5.09	5.19	5.18	5.07	5.26	6.5 ^b (XPS), 7 ^b (XES)
LiF	3.50	3.50	3.50	3.30	3.51	3.4 ^c (XPS)
MAE	0.59	0.68	0.64	1.08	0.65	
MSE	-0.24	0.31	0.16	0.81	0.18	

TABLE IV. QP valence bandwidths (in eV), at the WOT-SRSH and $G_0W_0@$ DFT level, for the various compounds and functionals under study. For zinc blende materials, the valence bandwidth is defined as the maximal energy difference between the top four (excluding spin degeneracy) valence bands. For the wurtzite and rock salt compounds, the valence bandwidth is defined as the maximal energy difference between the top three valence bands for LiF and MgO and the top six valence bands for AlN. At the bottom of the table are the MAE and MSE; all are in eV and calculated using the leftmost reported experimental values. Experimental data are obtained via XPS, angle-resolved photo-emission spectroscopy (ARPES), and X-ray emission spectroscopy (XES). Due to a lack of quality data on the contributions of ZPR in these results, we do not attempt to correct for such effects in our analysis.

a: [132], b: [133], c: [134]

	$G_0W_0@$	$G_0W_0@$	$G_0W_0@$	WOT-SRSH	$G_0W_0@$	Expt.
	PBE	PBE0	HSE		WOT-SRSH	
InSb	16.18	16.74	16.57	16.24	16.55	17.1 ^a , 16.98 ^b , 17.41 ^c
InAs	15.31	16.1	16.04	15.8	16.03	16.9 ^a , 17.40 ^c , 17.38 ^d
Ge	26.97	28.32	28.13	27.25	28.09	29.4 ^f
GaSb	17.12	15.52	18.15	17.52	18.11	18.8 ^a , 18.9 ^g
InP	14.86	15.71	15.57	15.37	15.55	17.1 ^a
GaAs	16.81	17.98	17.81	17.14	17.83	18.7 ^a , 18.7 ^b , 18.82 ^c
AlSb	29.68	30.66	30.5	30.05	30.55	31.15 ^e , 31.60 ^d
AlAs	36.66	37.97	37.82	37.56	38.03	39 ^h
GaP	16.03	17.2	17.03	16.64	17.02	18.6 ^a , 18.7 ^c
MAE	1.92	1.19	1.03	1.48	1.01	
MSE	-1.92	-1.19	-1.03	-1.48	-1.01	

TABLE V. QP highest d band positions, at the WOT-SRSH and $G_0W_0@$ DFT level, for the various functionals and d -electron containing compounds under study. At the bottom of the table are the MAE and MSE; all are in eV and measured relative to the leftmost reported experimental values. All experimental data are obtained via X-ray photo-emission spectroscopy (XPS). Due to a lack of quality data on the contributions of ZPR in these results, we do not attempt to correct for such effects in our analysis.

a: [135], b: [136], c: [137], d: [138], e: [139], f: [140], g: [141], h: [142]

IV.1.3. Bandwidths

The calculated valence bandwidths for all compounds are reported in Table IV. Additional results from DFT functionals other than WOT-SRSH can be found in the SI, section S-III.B [101]. For zinc blende materials, where there is strong sp^3 hybridization, the valence bandwidth is defined as the maximal energy difference between the top four (excluding spin degeneracy) valence bands. For the wurtzite and rock salt compounds, the valence bandwidth is defined as the maximal energy difference between the top three valence bands for LiF and MgO and the top six valence bands for AlN since it has twice as many atoms per unit cell. For more information on the states under consideration to compute bandwidths, see the leftmost column in Table IV. Unlike for QP band gaps, the effects of ZPR are not incorporated when comparing to experiment. Details on the DFT calculations (excluding WOT-SRSH) can be found in the SI. For

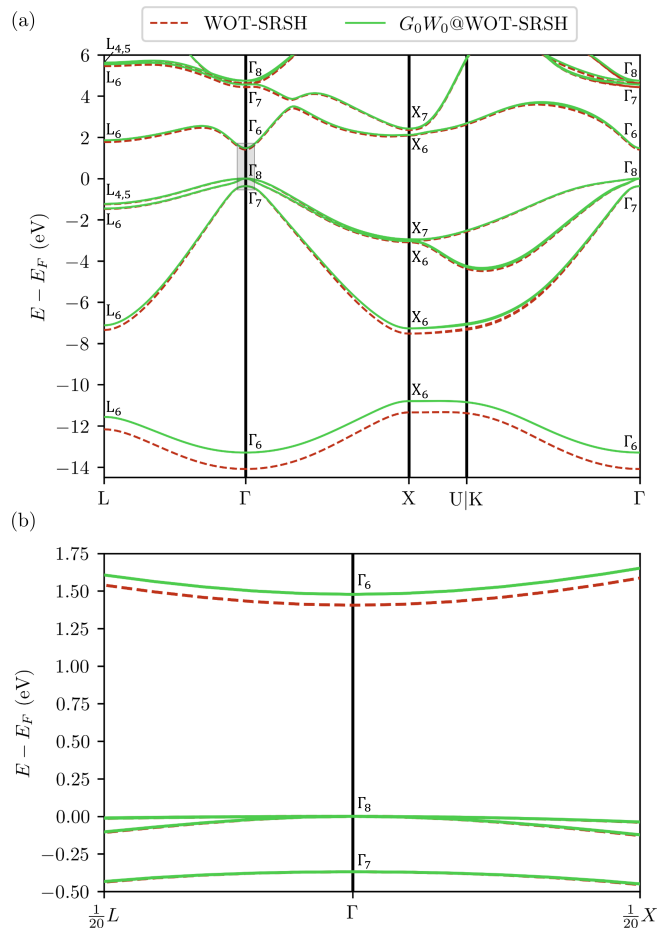


FIG. 2. Bandstructure of GaAs, including SOC, from WOT-SRSH and $G_0W_0@WOT-SRSH$. a) A full plot of the bandstructure, including the eight highest occupied orbitals and the first few eV of the next eight unoccupied orbitals. b) A zoomed-in inset—depicted by a gray box in a)—of the valence and conduction band extrema. For both plots, E_F is taken to be the energy of the valence band maxima

WOT-SRSH, the MAE and MSE are 1.08 and 0.81 eV respectively, suggesting the method tends to overestimate valence bandwidths by ~ 1 eV. $G_0W_0@WOT-SRSH$ has an MAE of 0.65 eV and an MSE of 0.18 eV, showing that G_0W_0 corrections away from the band gap offer a significant improvement in accuracy relative to WOT-SRSH. Notably, the valence bandwidths for the zinc blende compounds are generally overestimated relative to experiment by both WOT-SRSH and $G_0W_0@WOT-SRSH$, while for the rock salt compounds studied, the valence bandwidths are, if anything, underestimated.

Moving to the well-established starting point functionals, $G_0W_0@PBE$ computes bandwidths quite well, with an MAE of 0.59 eV and an MSE of -0.24 eV. It also tends to underestimate bandwidths as its MSE suggests. For hybrids, $G_0W_0@PBE0$ and $G_0W_0@HSE$ have MAEs of 0.68 and 0.64 eV and MSEs of 0.31 and 0.16 eV respectively. Interestingly, $G_0W_0@HSE$ and $G_0W_0@WOT-SRSH$ have comparable levels of accuracy for bandwidths. Unlike in the case of band gaps, this similar level of accuracy persists for wide-gap insulators.

IV.1.4. d Band Energies

For each semiconductor in our set that has elements for which d orbitals are explicitly treated as valence states, the d band position, defined as the highest d orbital eigen-energies relative to the valence band maxima, is reported in Table V. Additional results from DFT functionals other than WOT-SRSH can be found in the SI, section S-III.C [101]. As in the case of bandwidths, the effects of ZPR are not incorporated when comparing to experiment. For all calculations, we observe a universal underestimation of the d -orbital locations, making the distinction between the MAE and MSE meaningless. G_0W_0 corrections offer an improvement in accuracy for all starting points. For WOT-SRSH, the MSE decreases from 1.48 to 1.01 eV. For $G_0W_0@PBE$, it plummets from 3.8 to 1.92 eV. For $G_0W_0@PBE0$ it decreases from 1.7 to 1.19 eV, and for $G_0W_0@HSE$ it decreases from 1.47 to 1.03 eV. In total, $G_0W_0@HSE$ and $G_0W_0@WOT-SRSH$ appear to perform the best and offer a comparable level of accuracy. However, both methods still deviate from experimental reports by ~ 1 eV.

IV.2. Parameter Sensitivity of WOT-SRSH and $G_0W_0@WOT-SRSH$

The IP ansatz used to tune the range-separation parameter in the WOT-SRSH functional determines γ uniquely for a given choice of α and ε_∞ . However, there can be ambiguities in the selection of α and ε_∞ , with consequences for the predictive power of WOT-SRSH band gaps. Assuming first that ε_∞ has been computed accurately and that β is set to enforce $\alpha + \beta = \varepsilon_\infty^{-1}$, there exists, in principle, a range of choices of α for each material where one can find an optimal $\gamma > 0$ satisfying the

IP ansatz. These optimal (α, γ) pairs produce band gaps which can differ by up to a few hundred meV. Some of the ambiguity in selecting α is avoided by setting $\alpha = 0.25$ by default, but as discussed in Sec. II.1 an optimal γ cannot always be found when $\alpha = 0.25$, especially if $\varepsilon_\infty^{-1} \sim 0.25$. In such cases, α must be varied until it becomes possible to find an optimal γ which satisfies the IP ansatz and the constraint $\gamma > L^{-1}$, where L is the unit cell size used in the calculations. Additionally, it should be noted that while in principle α can be increased to be as large as 1, in practice values approaching unity are generally considered to be unphysically large for most systems [68]. Thus, WOT-SRSH predictions are, in practice, more precise than those one would obtain from considering the full range of α values.

Nonetheless, it is of significant interest to explore the ambiguity in selecting α in the WOT-SRSH framework further and its consequences for G_0W_0 @WOT-SRSH. To do so, we systematically vary α and γ and compute GKS and G_0W_0 QP band gaps for AlN. AlN is a good candidate for investigation since it has a dielectric constant that is very close to 0.25 and its band gap exhibits significant variation, on the order of hundreds of meV, between optimal (α, γ) pairs. The difference $\Delta E_g = E_g - E_{g,\text{ref}}$ between computed band gaps, relative to the chosen reference gaps $E_{g,\text{ref}}$ for SRSH and G_0W_0 @SRSH calculations of AlN, can be seen over a range of α and γ in Figure 3. Note that, as indicated, we are using, strictly speaking, the SRSH functional, as opposed to WOT-SRSH, meaning the IP ansatz is not satisfied for most of the data shown in Figure 3. The only overall constraint applied here is $\beta = \varepsilon_\infty^{-1} - \alpha$. Additionally, the G_0W_0 calculations presented here are slightly under-converged, using 256 bands to construct ε and Σ . Pairs of (α, γ) satisfying the IP ansatz are marked with black diamonds, and the reference band gap $E_{g,\text{ref}}$ is chosen to be the band gap obtained with the WOT-SRSH parameters of prior work [68] at either the DFT or G_0W_0 level. A range of ± 100 meV about this reference value is specified in white in the colormap.

Overall, G_0W_0 corrections to the SRSH starting point substantially reduce the sensitivity of the computed band gap to variations in α and γ by about a factor of 3. Specifically, at the SRSH level ΔE_g varies by 6.0 eV for the large ranges of α and γ considered, while for G_0W_0 @SRSH it varies by only 2.14 eV. This reduction in sensitivity becomes much more pronounced when only (α, γ) pairs satisfying the IP ansatz are considered. At the WOT-SRSH level, the ΔE_g values produced by these pairs have a range of 322 meV and depart from the white ± 100 meV range about $E_{g,\text{ref}}$ for the somewhat unphysical larger choices of α . In contrast, at the G_0W_0 @WOT-SRSH level, the exhibited range is only 26 meV. This reduction is by more than an order of magnitude, and substantially lower than the reduction observed for the overall SRSH functional. A similar set of trends is also observed for the other materials; see SI Section S-IV.1 [101].

We also note that there exists some uncertainty as to

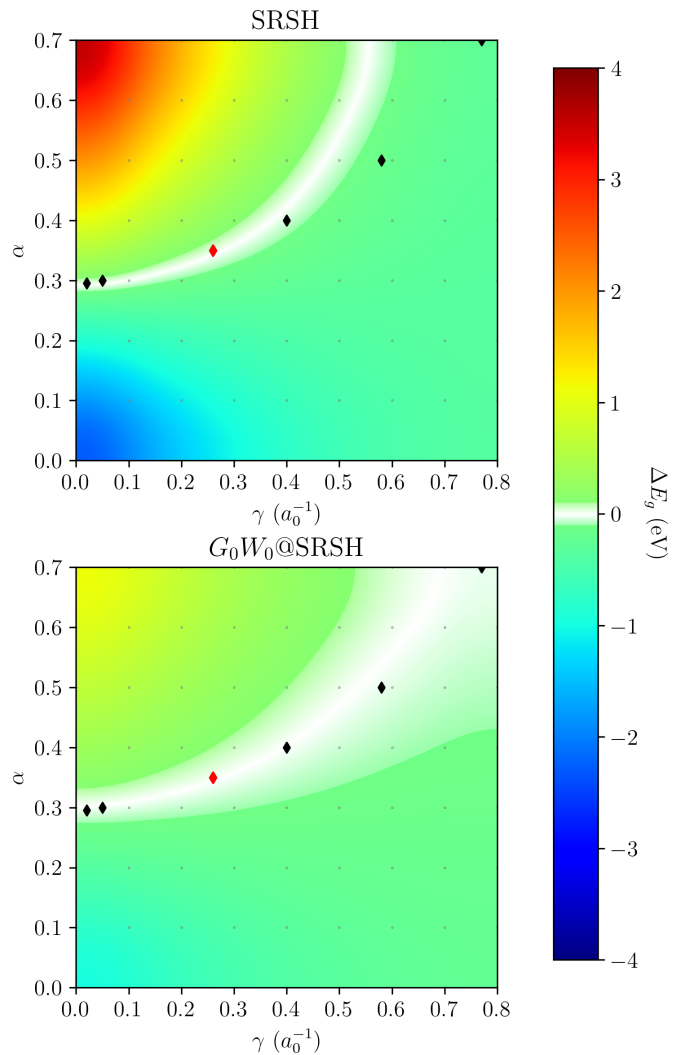


FIG. 3. The direct band gap of AlN, relative to a reference value ($\Delta E_g = E_g - E_{g,\text{ref}}$) at the SRSH and G_0W_0 @SRSH levels, interpolated over a wide range of (γ, α) values. The grid of performed calculations is represented as gray dots, and the pairs satisfying the WOT-SRSH constraint are depicted as diamonds, with the reference pair for ΔE_g in red. A range of ± 100 meV about the reference is shaded in white. G_0W_0 can be seen to suppress the overall variation at the SRSH level by about a factor of 3. Moreover, the pairs satisfying the WOT-SRSH constraint can be seen to leave the ± 100 meV range for the somewhat unphysically large values of α for SRSH, but not for G_0W_0 @SRSH.

how to select the long-range screening $\alpha + \beta = \varepsilon_\infty^{-1}$. For example, one could compute ε_∞ by considering the head of the RPA dielectric matrix used in GW [5]. However, the response to a finite electric field can also be employed, leading to a beyond-RPA value of ε_∞ [143, 144]. The inclusion of local field effects for such methods can also significantly affect the calculated response [145]. Additionally, the underlying DFT functional affects the computed ε_∞ . In fact, it is even possible to self-consistently update the value of $\alpha + \beta$ in an SRSH functional so that it matches the value obtained from a calculation of the di-

electric constant using said updated functional [41, 146].

Accordingly, we consider the effects of varying the dielectric constant for AlN. For the WOT-SRSH functional used here, ϵ_∞ was computed in prior work [68] via finite electric fields using a PBE0 functional. In lieu of re-computing the optimal γ value for different values of ϵ_∞ , we simply consider the effects of changing ϵ_∞ by $\pm 10\%$ while keeping α and γ fixed. This choice likely exacerbates the sensitivity of the functional because the IP ansatz is slightly violated for the values of ϵ_∞ which differ from the original one used to tune γ . As can be seen in Section S-IV.2 of the SI [101], these perturbations in ϵ_∞ result in the band gap changing by 260 meV at the SRSH level but only 80 meV at the G_0W_0 @SRSH level. This behavior is in line with the approximately three-fold band gap range flattening observed above. A similar trend is also observed for the other materials considered in the SI, Section S-IV.2 [101].

V. CONCLUSIONS

We have shown that a new WOT-SRSH class of range-separated hybrid functionals, which is tuned to satisfy an IP ansatz for localized orbitals and to have the correct asymptotic boundary conditions of the Coulomb potential in solids, offers an excellent starting point for G_0W_0 calculations of the electronic structure for a wide range of semiconductors and insulators. G_0W_0 @WOT-SRSH calculations perform at a level of accuracy that is equal to or better than state-of-the-art *evGW* and *QSGW* calculations at a lower computational cost. Additionally,

G_0W_0 @WOT-SRSH tends to improve the description of states deeper in the valence band manifold, leading to more accurate valence bandwidths and *d* band locations. Finally, we have shown that G_0W_0 @WOT-SRSH corrections greatly reduce the sensitivity of computed band gaps to variations in the underlying WOT-SRSH parameters that can arise from ambiguities in the optimal tuning procedure. In total, these calculations demonstrate that pairing WOT-SRSH with single-shot G_0W_0 methods offers a high-accuracy predictive method for calculating QP properties of materials with a wide range of band gaps.

ACKNOWLEDGEMENTS

This work was supported via US-Israel NSF-Binational Science Foundation (BSF) Grant DMR-2015991. Computational resources were provided by the Extreme Science and Engineering Discovery Environment (XSEDE) [147] supercomputer Stampede2 at the Texas Advanced Computing Center (TACC) through Grant No. TG-DMR190070, and additional computational resources were provided by the National Energy Research Scientific Computing Center (NERSC), DOE Office of Science User Facilities supported by the Office of Science of the US Department of Energy under Contract DE-AC02-05CH11231. MRF acknowledges support from the UK Engineering and Physical Sciences Research Council (EPSRC), grant no. EP/V010840/1, and LK thanks the Aryeh and Mintzi Katzman Professorial Chair and the Helen and Martin Kimmel Award for Innovative Investigation.

-
- [1] L. Hedin, Phys. Rev. **139**, A796 (1965).
 - [2] L. Hedin and S. Lundqvist, in *Solid State Physics*, Vol. 23, edited by F. Seitz, D. Turnbull, and H. Ehrenreich (Academic Press, 1970) pp. 1–181.
 - [3] G. Strinati, H. J. Mattausch, and W. Hanke, Phys. Rev. Lett. **45**, 290 (1980).
 - [4] G. Strinati, H. J. Mattausch, and W. Hanke, Phys. Rev. B **25**, 2867 (1982).
 - [5] M. S. Hybertsen and S. G. Louie, Phys. Rev. Lett. **55**, 1418 (1985).
 - [6] M. S. Hybertsen and S. G. Louie, Phys. Rev. B **34**, 5390 (1986).
 - [7] R. W. Godby, M. Schlüter, and L. J. Sham, Phys. Rev. Lett. **56**, 2415 (1986).
 - [8] F. Aryasetiawan and O. Gunnarsson, Rep. Prog. Phys. **61**, 237 (1998).
 - [9] W. G. Aulbur, L. Jönsson, and J. W. Wilkins, in *Solid State Physics*, Vol. 54, edited by H. Ehrenreich and F. Spaepen (Academic Press, 2000) pp. 1–218.
 - [10] R. M. Martin, *Electronic Structure: Basic Theory and Practical Methods*, 2nd ed. (Cambridge University Press, 2020).
 - [11] G. Onida, L. Reining, and A. Rubio, Rev. Mod. Phys. **74**, 601 (2002).
 - [12] F. Bruneval and M. A. L. Marques, J. Chem. Theory Comput. **9**, 324 (2013).
 - [13] C. Faber, P. Boulanger, C. Attaccalite, I. Duchemin, and X. Blase, Philos. Trans. Royal Soc. A **372**, 20130271 (2014).
 - [14] R. M. Martin, L. Reining, and D. M. Ceperley, *Interacting Electrons: Theory and Computational Approaches* (Cambridge University Press, Cambridge, 2016).
 - [15] L. Reining, Wiley Interdiscip. Rev. Comput. Mol. Sci. **8**, e1344 (2018).
 - [16] D. Golze, M. Dvorak, and P. Rinke, Front. Chem. **7**, 377 (2019).
 - [17] A. Seidl, A. Görling, P. Vogl, J. A. Majewski, and M. Levy, Phys. Rev. B **53**, 3764 (1996).
 - [18] P. Hohenberg and W. Kohn, Phys. Rev. **136**, B864 (1964).
 - [19] J. P. Perdew, K. Burke, and M. Ernzerhof, Phys. Rev. Lett. **77**, 3865 (1996).
 - [20] F. Fuchs, J. Furthmüller, F. Bechstedt, M. Shishkin, and G. Kresse, Phys. Rev. B **76**, 115109 (2007).
 - [21] T. Körzdörfer and N. Marom, Phys. Rev. B **86**, 041110(R) (2012).
 - [22] V. Atalla, M. Yoon, F. Caruso, P. Rinke, and M. Scheffler, Phys. Rev. B **88**, 165122 (2013).

- [23] S. Refaely-Abramson, S. Sharifzadeh, N. Govind, J. Autschbach, J. B. Neaton, R. Baer, and L. Kronik, *Phys. Rev. Lett.* **109**, 226405 (2012).
- [24] M. Dauth, F. Caruso, S. Kümmel, and P. Rinke, *Phys. Rev. B* **93**, 121115(R) (2016).
- [25] J. W. Knight, X. Wang, L. Gallandi, O. Dolgounitcheva, X. Ren, J. V. Ortiz, P. Rinke, T. Körzdörfer, and N. Marom, *J. Chem. Theory Comput.* **12**, 615 (2016).
- [26] N. Marom, *J. Phys.: Condens. Matter* **29**, 103003 (2017).
- [27] L. Leppert, T. Rangel, and J. B. Neaton, *Phys. Rev. Materials* **3**, 103803 (2019).
- [28] M. Hellgren, L. Baguet, M. Calandra, F. Mauri, and L. Wirtz, *Phys. Rev. B* **103**, 075101 (2021).
- [29] T. Rangel, M. Del Ben, D. Varsano, G. Antonius, F. Bruneval, F. H. da Jornada, M. J. van Setten, O. K. Orhan, D. D. O'Regan, A. Canning, A. Ferretti, A. Marini, G.-M. Rignanese, J. Deslippe, S. G. Louie, and J. B. Neaton, *Comput. Phys. Commun.* **255**, 107242 (2020).
- [30] M. P. Surh, S. G. Louie, and M. L. Cohen, *Phys. Rev. B* **43**, 9126 (1991).
- [31] W.-D. Schöne and A. G. Eguluz, *Phys. Rev. Lett.* **81**, 1662 (1998).
- [32] W. Luo, S. Ismail-Beigi, M. L. Cohen, and S. G. Louie, *Phys. Rev. B* **66**, 195215 (2002).
- [33] S. V. Faleev, M. van Schilfgaarde, and T. Kotani, *Phys. Rev. Lett.* **93**, 126406 (2004).
- [34] M. van Schilfgaarde, T. Kotani, and S. Faleev, *Phys. Rev. Lett.* **96**, 226402 (2006).
- [35] M. Shishkin and G. Kresse, *Phys. Rev. B* **75**, 235102 (2007).
- [36] T. Kotani, M. van Schilfgaarde, and S. V. Faleev, *Phys. Rev. B* **76**, 165106 (2007).
- [37] M. Shishkin, M. Marsman, and G. Kresse, *Phys. Rev. Lett.* **99**, 246403 (2007).
- [38] A. Kutepov, S. Y. Savrasov, and G. Kotliar, *Phys. Rev. B* **80**, 041103(R) (2009).
- [39] S. Refaely-Abramson, S. Sharifzadeh, M. Jain, R. Baer, J. B. Neaton, and L. Kronik, *Phys. Rev. B* **88**, 081204(R) (2013).
- [40] D. A. Egger, S. Weissman, S. Refaely-Abramson, S. Sharifzadeh, M. Dauth, R. Baer, S. Kümmel, J. B. Neaton, E. Zojer, and L. Kronik, *J. Chem. Theory Comput.* **10**, 1934 (2014).
- [41] J. H. Skone, M. Govoni, and G. Galli, *Phys. Rev. B* **89**, 195112 (2014).
- [42] L. Gallandi and T. Körzdörfer, *J. Chem. Theory Comput.* **11**, 5391 (2015).
- [43] L. Gallandi, N. Marom, P. Rinke, and T. Körzdörfer, *J. Chem. Theory Comput.* **12**, 605 (2016).
- [44] H. Jiang and P. Blaha, *Phys. Rev. B* **93**, 115203 (2016).
- [45] A. L. Kutepov, *Phys. Rev. B* **94**, 155101 (2016).
- [46] F. Caruso, M. Dauth, M. J. van Setten, and P. Rinke, *J. Chem. Theory Comput.* **12**, 5076 (2016).
- [47] J. Bois and T. Körzdörfer, *J. Chem. Theory Comput.* **13**, 4962 (2017).
- [48] A. L. Kutepov, *Phys. Rev. B* **95**, 195120 (2017).
- [49] M. Grumet, P. Liu, M. Kaltak, J. Klimeš, and G. Kresse, *Phys. Rev. B* **98**, 155143 (2018).
- [50] W. Li, V. Vlcek, H. Eisenberg, E. Rabani, R. Baer, and D. Neuhauser, arXiv:2102.11041 [cond-mat] (2021), arXiv:2102.11041 [cond-mat].
- [51] W. Chen and A. Pasquarello, *Phys. Rev. B* **92**, 041115(R) (2015).
- [52] M. J. van Setten, M. Giantomassi, X. Gonze, G.-M. Rignanese, and G. Hautier, *Phys. Rev. B* **96**, 155207 (2017).
- [53] N. Marom, F. Caruso, X. Ren, O. T. Hofmann, T. Körzdörfer, J. R. Chelikowsky, A. Rubio, M. Scheffler, and P. Rinke, *Phys. Rev. B* **86**, 245127 (2012).
- [54] S. Sharifzadeh, *J. Phys.: Condens. Matter* **30**, 153002 (2018).
- [55] P. Rinke, A. Qteish, J. Neugebauer, C. Freysoldt, and M. Scheffler, *New J. Phys.* **7**, 126 (2005).
- [56] F. Bruneval, N. Vast, and L. Reining, *Phys. Rev. B* **74**, 045102 (2006).
- [57] P. Liao and E. A. Carter, *Phys. Chem. Chem. Phys.* **13**, 15189 (2011).
- [58] L. Y. Isseroff and E. A. Carter, *Phys. Rev. B* **85**, 235142 (2012).
- [59] H. Jiang, R. I. Gomez-Abal, P. Rinke, and M. Scheffler, *Phys. Rev. B* **82**, 045108 (2010).
- [60] P. Rinke, A. Qteish, J. Neugebauer, and M. Scheffler, *Phys. Status Solidi B* **245**, 929 (2008).
- [61] N. Marom, X. Ren, J. E. Moussa, J. R. Chelikowsky, and L. Kronik, *Phys. Rev. B* **84**, 195143 (2011).
- [62] D. Lüftner, S. Refaely-Abramson, M. Pachler, R. Resel, M. G. Ramsey, L. Kronik, and P. Puschnig, *Phys. Rev. B* **90**, 075204 (2014).
- [63] C. Adamo and V. Barone, *J. Chem. Phys.* **110**, 6158 (1999).
- [64] A. V. Krukau, O. A. Vydrov, A. F. Izmaylov, and G. E. Scuseria, *J. Chem. Phys.* **125**, 224106 (2006).
- [65] T. Stein, H. Eisenberg, L. Kronik, and R. Baer, *Phys. Rev. Lett.* **105**, 266802 (2010).
- [66] M. Levy, J. P. Perdew, and V. Sahni, *Phys. Rev. A* **30**, 2745 (1984).
- [67] C.-O. Almbladh and U. von Barth, *Phys. Rev. B* **31**, 3231 (1985).
- [68] D. Wing, G. Ohad, J. B. Haber, M. R. Filip, S. E. Gant, J. B. Neaton, and L. Kronik, *PNAS* **118**, e2104556118 (2021).
- [69] J. Ma and L.-W. Wang, *Sci. Rep.* **6**, 24924 (2016).
- [70] T. Rangel, S. M. Hamed, F. Bruneval, and J. B. Neaton, *J. Chem. Theory Comput.* **12**, 2834 (2016).
- [71] T. Rangel, S. M. Hamed, F. Bruneval, and J. B. Neaton, *J. Chem. Phys.* **146**, 194108 (2017).
- [72] T. Yanai, D. P. Tew, and N. C. Handy, *Chem. Phys. Lett.* **393**, 51 (2004).
- [73] L. Kronik and J. B. Neaton, *Annu. Rev. Phys. Chem.* **67**, 587 (2016).
- [74] L. Kronik and S. Kümmel, *Adv. Mater.* **30**, 1706560 (2018).
- [75] J. P. Perdew, M. Ernzerhof, and K. Burke, *J. Chem. Phys.* **105**, 9982 (1996).
- [76] M. Ernzerhof and G. E. Scuseria, *J. Chem. Phys.* **110**, 5029 (1999).
- [77] J. Heyd, J. E. Peralta, G. E. Scuseria, and R. L. Martin, *J. Chem. Phys.* **123**, 174101 (2005).
- [78] J. Heyd, G. E. Scuseria, and M. Ernzerhof, *J. Chem. Phys.* **124**, 219906 (2006).
- [79] T. B. de Queiroz and S. Kümmel, *J. Chem. Phys.* **141**, 084303 (2014).
- [80] S. Bhandari, M. S. Cheung, E. Geva, L. Kronik, and B. D. Dunietz, *J. Chem. Theory Comput.* **14**, 6287 (2018).
- [81] J. P. Perdew, R. G. Parr, M. Levy, and J. L. Balduz, *Phys. Rev. Lett.* **49**, 1691 (1982).

- [82] J. P. Perdew and M. Levy, Phys. Rev. Lett. **51**, 1884 (1983).
- [83] L. J. Sham and M. Schlüter, Phys. Rev. Lett. **51**, 1888 (1983).
- [84] A. J. Cohen, P. Mori-Sánchez, and W. Yang, Phys. Rev. B **77**, 115123 (2008).
- [85] S. Kümmel and L. Kronik, Rev. Mod. Phys. **80**, 3 (2008).
- [86] J. P. Perdew, W. Yang, K. Burke, Z. Yang, E. K. U. Gross, M. Scheffler, G. E. Scuseria, T. M. Henderson, I. Y. Zhang, A. Ruzsinszky, H. Peng, J. Sun, E. Trushin, and A. Görling, PNAS **114**, 2801 (2017).
- [87] S. L. Adler, Phys. Rev. **126**, 413 (1962).
- [88] N. Wiser, Phys. Rev. **129**, 62 (1963).
- [89] R. W. Godby and R. J. Needs, Phys. Rev. Lett. **62**, 1169 (1989).
- [90] A. Oshlies, R. W. Godby, and R. J. Needs, Phys. Rev. B **51**, 1527 (1995).
- [91] M. Giantomassi, M. Stankovski, R. Shaltaf, M. Grüning, F. Bruneval, P. Rinke, and G.-M. Rignanese, Phys. Status Solidi B **248**, 275 (2011).
- [92] P. Liu, M. Kaltak, J. Klimeš, and G. Kresse, Phys. Rev. B **94**, 165109 (2016).
- [93] J. Wilhelm, M. Del Ben, and J. Hutter, J. Chem. Theory Comput. **12**, 3623 (2016).
- [94] O. Madelung, *Semiconductors: Data Handbook* (Springer Berlin Heidelberg, Berlin, Heidelberg, 2004).
- [95] K. Recker, F. Wallrafen, and K. Dupré, Naturwissenschaften **75**, 156 (1988).
- [96] H. Schulz and K. H. Thiemann, Solid State Commun. **23**, 815 (1977).
- [97] P. Giannozzi, S. Baroni, N. Bonini, M. Calandra, R. Car, C. Cavazzoni, D. Ceresoli, G. L. Chiarotti, M. Cococcioni, I. Dabo, *et al.*, J. Phys.: Condens. Matter **21**, 395502 (2009).
- [98] P. Giannozzi, O. Andreussi, T. Brumme, O. Bunau, M. Buongiorno Nardelli, M. Calandra, R. Car, C. Cavazzoni, D. Ceresoli, M. Cococcioni, *et al.*, J. Phys.: Condens. Matter **29**, 465901 (2017).
- [99] P. Giannozzi, O. Baseggio, P. Bonfà, D. Brunato, R. Car, I. Carnimeo, C. Cavazzoni, S. de Gironcoli, P. Delugas, F. Ferrari Ruffino, *et al.*, J. Chem. Phys. **152**, 154105 (2020).
- [100] L. Lin, J. Chem. Theory Comput. **12**, 2242 (2016).
- [101] See Supplemental Information at [URL will be inserted by publisher] for more technical details on calculations, results for standard DFT functionals, and additional parameter sensitivity results.
- [102] D. R. Hamann, Phys. Rev. B **88**, 085117 (2013).
- [103] M. J. van Setten, M. Giantomassi, E. Bousquet, M. J. Verstraete, D. R. Hamann, X. Gonze, and G. M. Rignanese, Comput. Phys. Commun. **226**, 39 (2018).
- [104] M. Rohlfing, P. Krüger, and J. Pollmann, Phys. Rev. Lett. **75**, 3489 (1995).
- [105] M. L. Tiago, S. Ismail-Beigi, and S. G. Louie, Phys. Rev. B **69**, 125212 (2004).
- [106] A. Fleszar and W. Hanke, Phys. Rev. B **71**, 045207 (2005).
- [107] J. Deslippe, G. Samsonidze, D. A. Strubbe, M. Jain, M. L. Cohen, and S. G. Louie, Comput. Phys. Commun. **183**, 1269 (2012).
- [108] P. Larson, M. Dvorak, and Z. Wu, Phys. Rev. B **88**, 125205 (2013).
- [109] A. Miglio, D. Waroquiers, G. Antonius, M. Giantomassi, M. Stankovski, M. Côté, X. Gonze, and G. M. Rignanese, Eur. Phys. J. B **85**, 322 (2012).
- [110] R. Laasner, J. Phys.: Condens. Matter **26**, 125503 (2014).
- [111] J. Deslippe, G. Samsonidze, M. Jain, M. L. Cohen, and S. G. Louie, Phys. Rev. B **87**, 165124 (2013).
- [112] B. D. Malone and M. L. Cohen, J. Phys.: Condens. Matter **25**, 105503 (2013).
- [113] B. A. Barker, *Electronic and Optical Properties of Solids with Strong Spin-Orbit Coupling*, Ph.D. thesis, UC Berkeley (2018).
- [114] D. Wing, J. B. Haber, R. Noff, B. Barker, D. A. Egger, A. Ramasubramaniam, S. G. Louie, J. B. Neaton, and L. Kronik, Phys. Rev. Materials **3**, 064603 (2019).
- [115] A. A. Mostofi, J. R. Yates, G. Pizzi, Y.-S. Lee, I. Souza, D. Vanderbilt, and N. Marzari, Comput. Phys. Commun. **185**, 2309 (2014).
- [116] I. Vurgaftman, J. R. Meyer, and L. R. Ram-Mohan, J. Appl. Phys. **89**, 5815 (2001).
- [117] C. D. Clark, P. J. Dean, P. V. Harris, and W. C. Price, Proc. R. Soc. Lond. A **277**, 312 (1964).
- [118] R. C. Whited, C. J. Flaten, and W. C. Walker, Solid State Commun. **13**, 1903 (1973).
- [119] M. Piacentini, Solid State Commun. **17**, 697 (1975).
- [120] M. Cardona and M. L. W. Thewalt, Rev. Mod. Phys. **77**, 1173 (2005).
- [121] S. Poncé, Y. Gillet, J. Laflamme Janssen, A. Marini, M. Verstraete, and X. Gonze, J. Chem. Phys. **143**, 102813 (2015).
- [122] W. Chen, G. Miceli, G.-M. Rignanese, and A. Pasquarello, Phys. Rev. Materials **2**, 073803 (2018).
- [123] J. P. Nery, P. B. Allen, G. Antonius, L. Reining, A. Miglio, and X. Gonze, Phys. Rev. B **97**, 115145 (2018).
- [124] F. Giustino, S. G. Louie, and M. L. Cohen, Phys. Rev. Lett. **105**, 265501 (2010).
- [125] E. Cannuccia and A. Marini, Phys. Rev. Lett. **107**, 255501 (2011).
- [126] S. Botti and M. A. L. Marques, Phys. Rev. Lett. **110**, 226404 (2013).
- [127] G. Antonius, S. Poncé, P. Boulanger, M. Côté, and X. Gonze, Phys. Rev. Lett. **112**, 215501 (2014).
- [128] H. Kawai, K. Yamashita, E. Cannuccia, and A. Marini, Phys. Rev. B **89**, 085202 (2014).
- [129] E. Maggio and G. Kresse, J. Chem. Theory Comput. **13**, 4765 (2017).
- [130] P. S. Schmidt, C. E. Patrick, and K. S. Thygesen, Phys. Rev. B **96**, 205206 (2017).
- [131] A. L. Kutepov, Phys. Rev. B **105**, 045124 (2022).
- [132] A. Goldmann and E.-E. Koch, eds., *Subvolume A, Landolt-Börnstein - Group III Condensed Matter*, Vol. 23a (Springer-Verlag, Berlin/Heidelberg, 1989).
- [133] S. P. Kowalczyk, F. R. McFeely, L. Ley, V. T. Gritsyna, and D. A. Shirley, Solid State Commun. **23**, 161 (1977).
- [134] C.-u. Ro and R. W. Linton, Surf. Sci. Spectra **1**, 277 (1992).
- [135] N. J. Shevchik, J. Tejada, and M. Cardona, Phys. Rev. B **9**, 2627 (1974).
- [136] M. Cardona, C. M. Pechina, N. J. Shevchik, and J. Tejada, Solid State Commun. **11**, 1655 (1972).
- [137] L. Ley, R. A. Pollak, F. R. McFeely, S. P. Kowalczyk, and D. A. Shirley, Phys. Rev. B **9**, 600 (1974).
- [138] J. R. Waldrop, G. J. Sullivan, R. W. Grant, E. A. Kraut, and W. A. Harrison, J. Vac. Sci. Technol. B **10**, 1773 (1992).

- [139] D. H. Ehlert, F. U. Hillebrecht, C. T. Lin, E. Schönherr, and L. Ley, *Phys. Rev. B* **40**, 3812 (1989).
- [140] E. A. Kraut, R. W. Grant, J. R. Waldrop, and S. P. Kowalczyk, *Phys. Rev. B* **28**, 1965 (1983).
- [141] G. J. Gualtieri, G. P. Schwartz, R. G. Nuzzo, and W. A. Sunder, *Appl. Phys. Lett.* **49**, 1037 (1986).
- [142] H. Okumura, I. Yoshida, S. Misawa, and S. Yoshida, *J. Vac. Sci. Technol. B* **5**, 1622 (1987).
- [143] R. W. Nunes and X. Gonze, *Phys. Rev. B* **63**, 155107 (2001).
- [144] I. Souza, J. Íñiguez, and D. Vanderbilt, *Phys. Rev. Lett.* **89**, 117602 (2002).
- [145] J. E. Northrup, M. S. Hybertsen, and S. G. Louie, *Phys. Rev. Lett.* **59**, 819 (1987).
- [146] J. H. Skone, M. Govoni, and G. Galli, *Phys. Rev. B* **93**, 235106 (2016).
- [147] J. Towns, T. Cockerill, M. Dahan, I. Foster, K. Gaither, A. Grimshaw, V. Hazlewood, S. Lathrop, D. Lifka, G. D. Peterson, *et al.*, *Comput Sci Eng* **16**, 62 (2014).

An Optimally-Tuned Starting Point for Single-Shot *GW* Calculations of Solids: *Supplementary Information*

Stephen E. Gant,¹ Jonah B. Haber,¹ Marina R. Filip,² Francisca Sagredo,¹
Dahvyd Wing,³ Guy Ohad,³ Leeor Kronik,³ and Jeffrey B. Neaton^{4,5,6}

¹*Department of Physics, University of California,
Berkeley, Berkeley, California 94720, USA*

²*Department of Physics, University of Oxford,
Clarendon Laboratory, Oxford OX1 3PU, United Kingdom*

³*Department of Molecular Chemistry and Materials Science,
Weizmann Institute of Science, Rehovoth 76100, Israel*

⁴*Department of Physics, University of California,
Berkeley, Berkeley, California 94720, USA*

⁵*Materials Sciences Division, Lawrence Berkeley National Laboratory, Berkeley, California 94720, USA*

⁶*Kavli Energy NanoScience Institute at Berkeley, Berkeley, California 94720, USA*

S-I. NON-SELF-CONSISTENT FIELD CALCULATIONS FOR HYBRID FUNCTIONALS

One roadblock for using hybrid functional starting points in QUANTUM ESPRESSO (QE) for MBPT calculations is that by default in QE (version 6.2), hybrid DFT can only be carried out self-consistently. More specifically, this involves two nested self-consistent field (SCF) loops. The inner loop converges the generalized Kohn-Sham (GKS) eigensystem while holding the exact exchange operator in the Hamiltonian fixed. Then, the outer loop constructs the exact exchange operator from the GKS system and checks for self-consistency. Naively, following QE's constraint that the computation of the exact exchange for $\mathcal{O}(10^3)$ states be done self-consistently requires approximately seven costly iterations. However, given a converged ground state density ρ and set of occupied orbitals $\{\phi_i\}_{i \in \text{occ}}$, only one iteration should be needed. As is well-known, the conventional DFT Hamiltonian is simply a functional of ρ . Moreover, the exact Fock exchange operator

$$V_X(\mathbf{r}, \mathbf{r}') = - \sum_{i \in \text{occ}} \frac{1}{|\mathbf{r} - \mathbf{r}'|} \phi_i^*(\mathbf{r}') \phi_i(\mathbf{r}) \quad (\text{S1})$$

only depends on the occupied orbitals. Because altering the number of unoccupied states under consideration will not alter the Hamiltonian, it should be possible to perform a non-self consistent field (NSCF) calculation using a converged density and set of occupied orbitals $\{\rho, \{\phi_i\}_{i \in \text{occ}}\}$ to obtain the unoccupied states needed for *GW*.

Another issue obstructing the aforementioned single iteration of exact exchange is that QE does not construct the exact exchange operator until a single inner SCF loop has been completed. This makes even simply re-running a calculation from a well-converged ground state density and set of occupied orbitals much more costly than it needs to be. The QE algorithm re-diagonalizes an incomplete Hamiltonian without exact exchange, altering the well-converged eigensystem, and necessitating about as many total SCF iterations to re-converge as one would need if the system had started from a completely unconverged $\{\rho, \{\phi_i\}_{i \in \text{occ}}\}$. Both of the above facts make performing a non-SCF (NSCF) calculation for the unoccupied bands (a common best practice in *GW*) impossible for hybrid functionals in QE.

To remedy these issues, we implemented a few alterations to our QE code and workflow. First, we permitted the exact exchange operator to be constructed before the first inner SCF loop. This means that a restarted hybrid functional calculation no longer pushes $\{\rho, \{\phi_i\}_{i \in \text{occ}}\}$ away from its converged state. Second, we modified the code to allow for explicit control of the number of exact exchange iterations performed. This was needed because QE will always perform at least two exact exchange iterations so that it can check for self-consistency in the outer SCF loop. However, if the eigensystem being fed in is already converged, the second iteration is unnecessary. Lastly, we devised a workaround which takes a converged ground state eigensystem $\{\rho, \{\phi_i\}_{i \in \text{occ}}\}$ and populates the desired number of unoccupied states in the saved many-body eigenfunction. These alterations allow for QE to accurately compute the new extended eigensystem, including $\mathcal{O}(10^3)$ unoccupied states, through a single SCF loop. In practice, we found this to reduce the cost of computing the unoccupied states for a *GW* calculation by about a factor of seven (the number of SCF loops usually required without the above modifications).

It should also be noted that even though conventional computation of the exact exchange operator does not depend on the unoccupied states, there is a small dependence observed in our work. When testing our modifications on Si we found that doubling the number of bands under consideration resulted in a change of $\sim 10 \mu\text{eV}$ in the computed band gap of Si. This is likely due to the fact that we are using adaptively compressed exchange (ACE) [S1] to handle the exact exchange. In this algorithm, the unoccupied states are formally incorporated in the construction of the compressed exchange operator. Moreover, the number of unoccupied states, especially those close to the Fermi level, have been shown to have a minor influence on the convergence of the exact exchange operator [S1]. Nonetheless, such a small change is negligible in comparison to the other sources of error under consideration.

S-II. GW CONVERGENCE

The convergence parameters used in the G_0W_0 calculations for each system can be found in Table S1. S-II.1 and S-II.2 provide an illustrative example for GaAs of the analysis used to determine the final convergence parameters of our G_0W_0 calculations. Due to the increased cost of hybrid functionals, convergence data were determined using the PBE functional [S2] for calculations. This example shows that based on the level of convergence of the number of q points, the dielectric cutoff, and the number of bands used in constructing ϵ and Σ , the G_0W_0 calculations for GaAs underestimate the its QP band gap by about 20 meV.

	# Bands	ϵ Cutoff (Ry)	k/q -grid
InSb	512	50	6x6x6
InAs	512	40	6x6x6
Ge	512	50	8x8x8
GaSb	512	60	8x8x8
Si	256	30	6x6x6
InP	256	40	6x6x6
GaAs	512	70	6x6x6
AlSb	256	40	6x6x6
AlAs	512	40	6x6x6
GaP	256	30	6x6x6
AlP	256	30	6x6x6
C	256	60	6x6x6
AlN	1024	50	7x7x4
MgO	512	60	6x6x6
LiF	1024	80	6x6x6

Table S1. *GW* convergence data for each system under study. The static remainder approximation for the self-energy is used for all systems in which it offered faster convergence with respect to the number of bands (i.e. all materials but AlN, MgO, and LiF). The number of bands (including both occupied and unoccupied states) used are chosen to be powers of 2 in order to maximize band parallelization efficiency.

S-II.1. Number of Bands and Dielectric Cutoff

Convergence of the direct band gap of GaAs at Γ with respect to the number of bands (used in both the construction of the polarizability and the self-energy) and the dielectric cutoff was performed simultaneously. This yielded dielectric cutoff convergence series for a variety of numbers of bands, as depicted in Figure S1. In order to extrapolate the limit of $E_{\varepsilon, \text{cutoff}} \rightarrow \infty$ the y intercept of the data series for $E_{\varepsilon, \text{cutoff}}^{-1}$ was considered. Our choice of $E_{\varepsilon, \text{cutoff}} = 70$ Ry and 512 bands for sufficiently converged parameters is expected to underestimate the fully converged gap by about 10 meV.

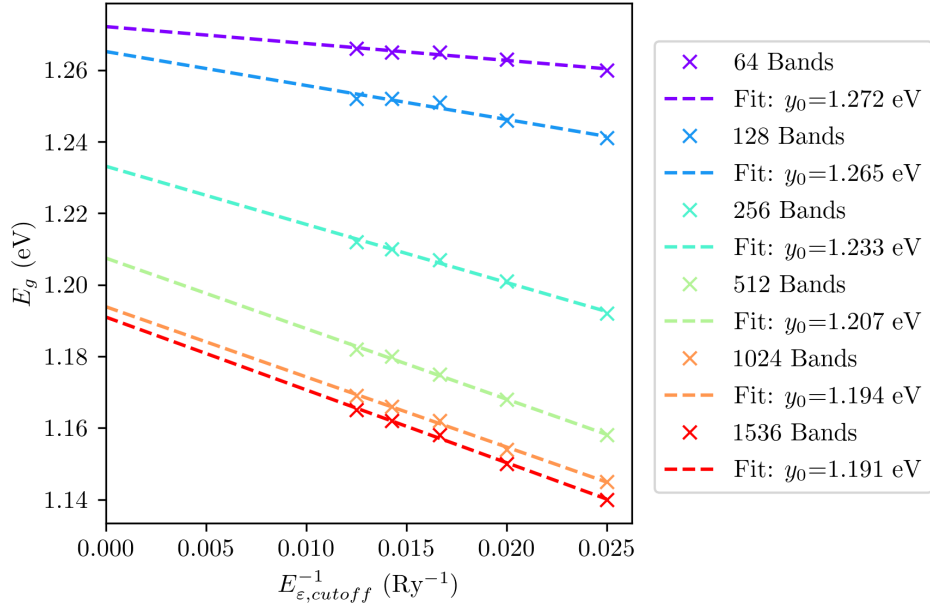


Figure S1. Convergence of the direct band gap of GaAs at Γ with respect to the number of bands and the dielectric cutoff. Dielectric cutoff convergence is extrapolated to infinity via a linear fit to the inverse cutoff $E_{\varepsilon, \text{cutoff}}^{-1}$. The y intercept of the fit, representing the $E_{\varepsilon, \text{cutoff}} \rightarrow \infty$ limit, is reported in the legend for varying number of bands.

S-II.2. q -grid

Using a half-shifted $10 \times 10 \times 10$ k -grid to obtain a well-converged ground state density at the PBE level, the convergence of the direct band gap of GaAs at Γ with respect to the number of q points used in constructing the dielectric response function was analyzed. Figure S2 (a) shows that while the band gap is still changing even at $N_q^{1/3} = 12$, it appears to be leveling off, and the choice of $N_q^{1/3} = 6$ yields a gap that is underestimating by 9 meV. Likewise, as seen in Figure S2 (b), a linear fit of the last three gaps as a function of N_q^{-1} shows an intercept at 1.235 eV, suggesting the choice of a $6 \times 6 \times 6$ q -grid underestimates the bands gap by 12 meV. From these considerations we conclude that the choice of a $6 \times 6 \times 6$ q -grid underestimates the band gap by about 10 meV.

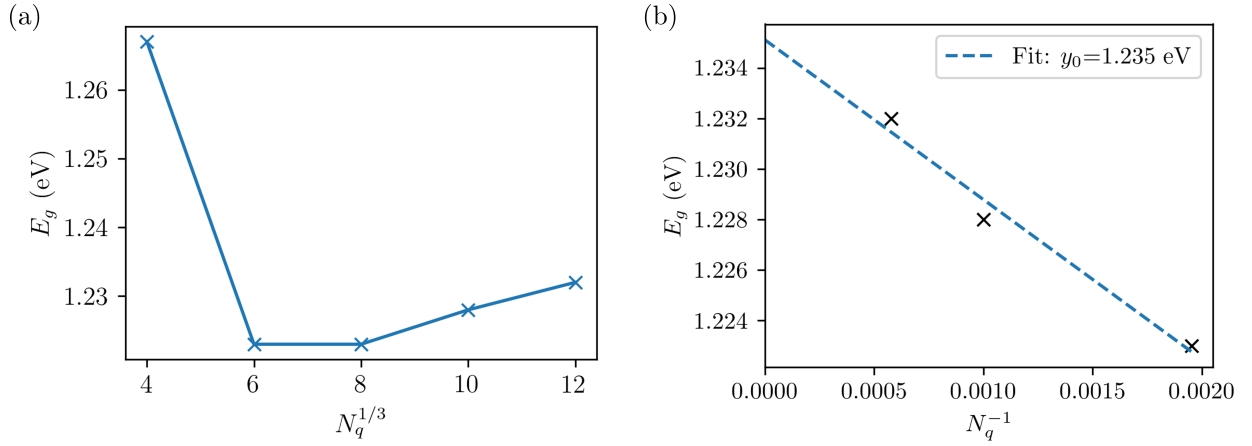


Figure S2. Convergence of the direct band gap of GaAs at Γ with respect to the number of q -points N_q used in constructing the dielectric response function. (a) shows the relationship with respect to $N_q^{1/3}$, and (b) shows the relationship with respect to N_q^{-1} .

S-III. DFT RESULTS

S-III.1. Band Gaps

	PBE	PBE0	HSE	Ref	ZPR
InSb	-0.45	0.83	0.28	0.19	0.17 ^a , 0.02 ^f
InAs	-0.35	0.91	0.38	0.37	0.35 ^a , 0.02 ^f
Ge	0.08	1.25	0.69	0.71	0.66 ^b , 0.05 ^f
GaSb	-0.12	1.22	0.69	0.76	0.73 ^a , 0.03 ^f
Si	0.55	1.77	1.12	1.18	1.12 ^b , 0.06 ^f
InP	0.69	2.09	1.48	1.40	1.35 ^a , 0.05 ^f
GaAs	0.40	1.86	1.27	1.47	1.42 ^a , 0.05 ^f
AlSb	0.99	2.14	1.52	1.65	1.61 ^a , 0.04 ^f
AlAs	1.33	2.61	1.96	2.20	2.16 ^a , 0.04 ^f
GaP	1.57	2.92	2.26	2.35	2.27 ^a , 0.08 ^f
AlP	1.56	2.91	2.24	2.51	2.49 ^a , 0.02 ^f
C	4.18	5.99	5.23	5.85	5.47 ^c , 0.38 ^g
AlN	4.22	6.27	5.57	6.52	6.14 ^a , 0.38 ^g
MgO	4.56	7.19	6.46	8.36	7.83 ^d , 0.53 ^h
LiF	9.08	12.14	11.40	15.35	14.20 ^e , 1.15 ^h
MAE	1.50	0.70	0.58		
MSE	-1.50	0.081	-0.56		
Max Error	-6.38	-3.20	-3.95		

Table S2. Additional band gaps (in eV) at the DFT level for the various compounds under study. At the bottom of the table are the MAE (mean absolute error), MSE (mean signed error), and Max Error; all are in eV and measured relative to the reported reference values, which are arrived at by incorporating ZPR corrections into experimental band gap data. Experimental results are arrived at via an analysis of optical absorption spectroscopy data, where excitonic effects are taken into account to arrive at the fundamental gap (See [S3] for details).

References: a: [S4], b: [S5], c: [S6], d: [S7], e: [S8], f: [S9], g: [S10], h: [S11, S12]

S-III.2. Valence Bandwidths

		PBE	HSE	PBE0	Expt.
InSb	$E_{\Gamma,8v} - E_{\Gamma,6v}$	10.97	12.05	12.17	11.7 ^a (XPS), 10.8 ^a (ARPES)
InAs	$E_{\Gamma,8v} - E_{\Gamma,6v}$	11.95	13.14	13.26	12.3 ^a (XPS)
Ge	$E_{\Gamma,8v} - E_{\Gamma,6v}$	12.87	14.19	14.32	12.6 ^a (XPS)
GaSb	$E_{\Gamma,8v} - E_{\Gamma,6v}$	11.79	12.96	13.09	11.6 ^a (XPS), 11.64 ^a (ARPES)
Si	$E_{\Gamma,8v} - E_{\Gamma,6v}$	11.98	13.30	13.40	12.5 ^a (XPS)
InP	$E_{\Gamma,8v} - E_{\Gamma,6v}$	11.53	12.74	12.83	11.0 ^a (XPS), 11.4 ^a (IPES)
GaAs	$E_{\Gamma,8v} - E_{\Gamma,6v}$	12.85	14.12	14.22	13.8 ^a (XPS), 13.1 ^a (ARPES)
AlSb	$E_{\Gamma,8v} - E_{\Gamma,6v}$	10.96	12.07	12.17	—
AlAs	$E_{\Gamma,8v} - E_{\Gamma,6v}$	11.97	13.19	13.28	—
GaP	$E_{\Gamma,8v} - E_{\Gamma,6v}$	12.52	13.81	13.90	12.5 ^a (ARPES)
AlP	$E_{\Gamma,8v} - E_{\Gamma,6v}$	11.52	12.76	12.83	—
C	$E_{\Gamma,8v} - E_{\Gamma,6v}$	21.50	23.7	23.74	21 ^a (XPS)
AlN	$E_{\Gamma,6v} - E_{L,3v}$	5.99	6.51	6.55	—
MgO	$E_{\Gamma,15v} - E_{L,1v}$	4.52	4.92	4.95	6.5 ^b (XPS), 7 ^b (XES)
LiF	$E_{\Gamma,15v} - E_{X,4v}$	3.00	3.14	3.16	3.4 ^c (XPS)
MAE		0.59	1.25	1.17	
MSE		-0.31	0.92	0.83	

Table S3. Valence bandwidths (in eV) at the DFT level for the compounds under study. For zinc blende materials, the valence bandwidth is defined as the maximal energy difference between the top four (excluding spin degeneracy) valence bands. For the wurtzite and rock salt compounds, the valence bandwidth is defined as the maximal energy difference between the top three valence bands for LiF and MgO and the top six valence bands for AlN. At the bottom of the table are the MAE and MSE; all are in eV and calculated using the leftmost reported experimental values. Experimental data are obtained via XPS, angle-resolved photoemission spectroscopy (ARPES), and X-ray emission spectroscopy (XES). Due to a lack of quality data on the contributions of ZPR in these results, we do not attempt to correct for such effects in our analysis.

References: a: [S13], b: [S14], c: [S15]

S-III.3. d Band Positions

	PBE	PBE0	HSE	Expt.
InSb	14.44	16.43	16.32	17.1 ^a , 16.98 ^b , 17.41 ^c
InAs	14.04	15.93	15.86	16.9 ^a , 17.40 ^c , 17.38 ^d
Ge	24.47	27.51	27.38	29.4 ^f
GaSb	15.04	14.83	17.62	18.8 ^a , 18.9 ^g
InP	13.73	15.56	15.48	17.1 ^a
GaAs	14.64	17.26	17.17	18.7 ^a , 18.7 ^b , 18.82 ^c
AlSb	27.86	30.14	30.06	31.15 ^e , 31.60 ^d
AlAs	34.18	37.12	37.05	39 ^h
GaP	14.28	16.81	16.73	18.6 ^a , 18.7 ^c
MAE	3.80	1.70	1.47	
MSE	-3.80	-1.70	-1.47	

Table S4. QP highest d band positions at the DFT level for the various compounds under study which contain d electrons. At the bottom of the table are the MAE and MSE; all are in eV and measured relative to the leftmost reported experimental values. All experimental data are obtained via X-ray photo-emission spectroscopy (XPS). Due to a lack of quality data on the contributions of ZPR in these results, we do not attempt to correct for such effects in our analysis.

References: a: [S16], b: [S17], c: [S18], d: [S19], e: [S20], f: [S21], g: [S22], h: [S23]

S-IV. SRSH AND G_0W_0 @SRSH SENSITIVITY

S-IV.1. α and γ variance for LiF and AIP

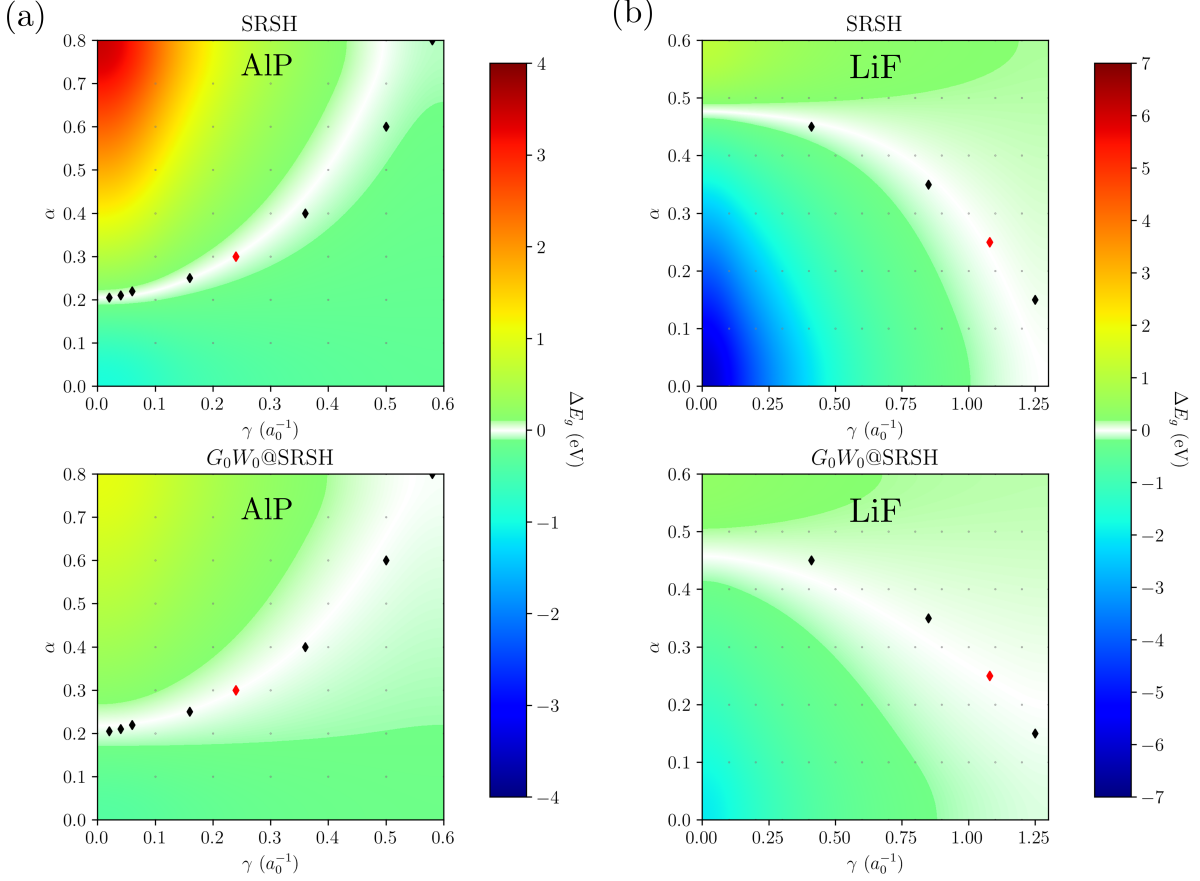


Figure S3. Direct band gaps of AIP (a) and LiF (b) relative to their reference value ($\Delta E_g = E_g - E_{\text{ref}}$) at the SRSH and G_0W_0 @SRSH levels, interpolated over a wide range of (γ, α) values. The grid of performed calculations is represented as gray dots, and the pairs satisfying the WOT-SRSH constraint are depicted as diamonds, with the reference pair for ΔE_g in red. A range of ± 100 meV about the reference point is shaded in white-green. G_0W_0 is seen to suppress the overall variation at the SRSH level by about a factor of three.

As discussed in the main text, the application of G_0W_0 based on a SRSH functional starting point suppresses how much the band gap relative to a reference value (red diamond) ΔE_g changes. Depicted in Figure S3 are the interpolated values of ΔE_g for AIP and LiF. Both compounds express similar trends to those reported for AlN in the main text. The sensitivity of ΔE_g is suppressed by about a factor of three, and the optimal (α, γ) pairs (shown as black crosses) tend to lie more tightly about the $\Delta E_g = 0$ line for G_0W_0 @SRSH.

One notable difference is that the optimal (α, γ) pairs for LiF have a negative slope, as opposed to AlN and AlP which have series with positive slopes. A similar slope-change trend has been observed in previous empirical tuning of SRSF functionals and tends to occur for small ϵ_∞ , wide-band-gap materials [S24].

S-IV.2. ϵ_∞ variance for AlN, AlSb, and LiF

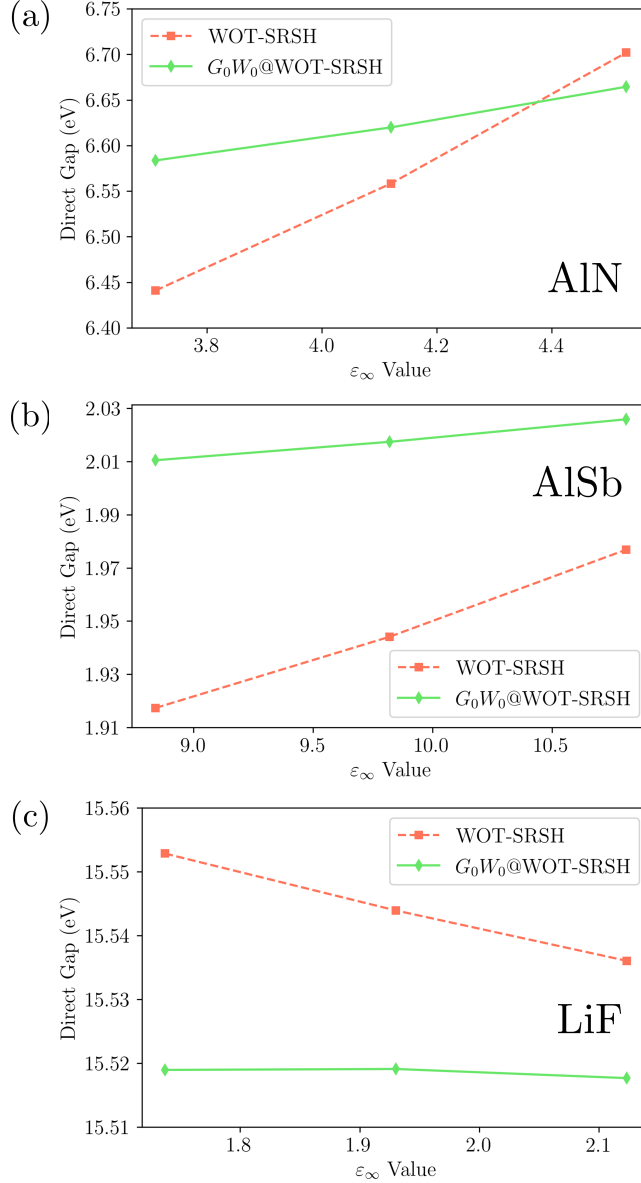


Figure S4. Band gaps for various materials at the SRSH and G_0W_0 @SRSH levels as ϵ_∞ is varied by $\pm 10\%$. G_0W_0 corrections suppress the variability in the band gaps by a factor of three for AlN, AlSb, and substantially more for than that for LiF.

-
- [S1] L. Lin, *J. Chem. Theory Comput.* **12**, 2242 (2016).
- [S2] J. P. Perdew, K. Burke, and M. Ernzerhof, *Phys. Rev. Lett.* **77**, 3865 (1996).
- [S3] D. Wing, G. Ohad, J. B. Haber, M. R. Filip, S. E. Gant, J. B. Neaton, and L. Kronik, *PNAS* **118**, e2104556118 (2021).
- [S4] I. Vurgaftman, J. R. Meyer, and L. R. Ram-Mohan, *J. Appl. Phys.* **89**, 5815 (2001).
- [S5] O. Madelung, *Semiconductors: Data Handbook* (Springer Berlin Heidelberg, Berlin, Heidelberg, 2004).
- [S6] C. D. Clark, P. J. Dean, P. V. Harris, and W. C. Price, *Proc. Math. Phys. Eng. Sci. P ROY SOC A-MATH PHY* **277**, 312 (1964).
- [S7] R. C. Whited, C. J. Flaten, and W. C. Walker, *Solid State Commun.* **13**, 1903 (1973).
- [S8] M. Piacentini, *Solid State Commun.* **17**, 697 (1975).
- [S9] M. Cardona and M. L. W. Thewalt, *Rev. Mod. Phys.* **77**, 1173 (2005).
- [S10] S. Poncé, Y. Gillet, J. Laflamme Janssen, A. Marini, M. Verstraete, and X. Gonze, *J. Chem. Phys.* **143**, 102813 (2015).
- [S11] W. Chen, G. Miceli, G.-M. Rignanese, and A. Pasquarello, *Phys. Rev. Materials* **2**, 073803 (2018).
- [S12] J. P. Nery, P. B. Allen, G. Antonius, L. Reining, A. Miglio, and X. Gonze, *Phys. Rev. B* **97**, 115145 (2018).
- [S13] A. Goldmann and E.-E. Koch, eds., *Subvolume A*, Landolt-Börnstein - Group III Condensed Matter, Vol. 23a (Springer-Verlag, Berlin/Heidelberg, 1989).
- [S14] S. P. Kowalczyk, F. R. McFeely, L. Ley, V. T. Gritsyna, and D. A. Shirley, *Solid State Commun.* **23**, 161 (1977).
- [S15] C.-u. Ro and R. W. Linton, *Surf. Sci. Spectra* **1**, 277 (1992).
- [S16] N. J. Shevchik, J. Tejada, and M. Cardona, *Phys. Rev. B* **9**, 2627 (1974).
- [S17] M. Cardona, C. M. Penchina, N. J. Shevchik, and J. Tejada, *Solid State Commun.* **11**, 1655 (1972).
- [S18] L. Ley, R. A. Pollak, F. R. McFeely, S. P. Kowalczyk, and D. A. Shirley, *Phys. Rev. B* **9**, 600 (1974).
- [S19] J. R. Waldrop, G. J. Sullivan, R. W. Grant, E. A. Kraut, and W. A. Harrison, *J. Vac. Sci. Technol. B* **10**, 1773 (1992).
- [S20] D. H. Ehlers, F. U. Hillebrecht, C. T. Lin, E. Schönherr, and L. Ley, *Phys. Rev. B* **40**, 3812 (1989).
- [S21] E. A. Kraut, R. W. Grant, J. R. Waldrop, and S. P. Kowalczyk, *Phys. Rev. B* **28**, 1965 (1983).
- [S22] G. J. Gualtieri, G. P. Schwartz, R. G. Nuzzo, and W. A. Sunder, *Appl. Phys. Lett.* **49**, 1037 (1986).
- [S23] H. Okumura, I. Yoshida, S. Misawa, and S. Yoshida, *J. Vac. Sci. Technol. B* **5**, 1622 (1987).
- [S24] J. H. Skone, M. Govoni, and G. Galli, *Phys. Rev. B* **93**, 235106 (2016).